

Sensitivity of Tropical Tropospheric Temperature to Sea Surface Temperature Forcing

Hui Su, J. David Neelin and Joyce E. Meyerson

August 29, 2002

Department of Atmospheric Sciences
and Institute of Geophysics and Planetary Physics
University of California, Los Angeles

Revised for *Journal of Climate*

Corresponding author address:

J. David Neelin

Department of Atmospheric Sciences

University of California, Los Angeles, Los Angeles, CA 90095-1565

e-mail: neelin@atmos.ucla.edu

Abstract

During El Niño, there are substantial tropospheric temperature anomalies across the entire tropical belt associated with the warming of sea surface temperature (SST) in the central and eastern Pacific. The quasi-equilibrium tropical circulation model (QTCM) is used to investigate the mechanisms for tropical tropospheric temperature response to SST forcing. In both observations and model simulations, the tropical-averaged tropospheric temperature anomaly $\langle \hat{T}' \rangle$ is approximately linear with tropical mean SST anomaly $\langle T'_s \rangle$ for observed SST forcing. Regional SST anomaly experiments are used to estimate regional sensitivity measures and quantify the degree of nonlinearity. For instance, SST anomalies of 3 C in the central Pacific would give a nonlinear $\langle \hat{T}' \rangle$ response about 15% greater than a linear fit to small SST anomaly experiments would predict but for the maximum observed SST anomaly in this region the response differs by only 5% from linearity. Nonlinearity in $\langle \hat{T}' \rangle$ response is modest even when local precipitation response is highly nonlinear. While temperature anomalies have large spatial scales, the main precipitation anomaly tends to be local to the SST anomaly regions. The tropical averaged precipitation anomalies bear no simple relation to tropical averaged tropospheric temperature anomalies or SST forcing. The approximate linearity of the $\langle \hat{T}' \rangle$ response is due to two factors: (1) the strong nonlinearities that occur locally tend to be associated with the transport terms which become small in the large-area average; and (2) the dependence on temperature of the top-of-atmosphere and surface fluxes has only weak nonlinearity over the range of $\langle \hat{T}' \rangle$ variations. Analytical approximations to the QTCM suggest that the direct impact of climatological SST, via flux terms, contributes modestly to regional variations in the sensitivity α of $\langle \hat{T}' \rangle$ to $\langle T'_s \rangle$. Wind speed has a fairly strong effect on α but tends to oppose the direct effect of SST since cold SST regions often have stronger climatological wind which would yield larger slopes. A substantial contribution to regional variation in α comes from the different reaction of moisture to SST anomalies in precipitating and non-precipitating regions. Although regions over climatologically warm water have a slightly higher sensitivity, subregions of El Niño SST anomalies even in the colder eastern Pacific contribute substantially to tropospheric temperature anomalies.

1 Introduction

During El Niño, there are substantial warm tropospheric temperature anomalies across the entire tropical band (Yulaeva and Wallace, 1994; Wallace et al., 1998) and vice versa for La Niña. Various measures of tropical temperature anomaly follow the variations of sea surface temperature (SST) in the eastern Pacific Ocean, with lags up to a few months (e.g. Newell and Weare 1976; Angell 1981; Horel and Wallace 1981; Pan and Oort 1983; Kumar and Hoerling 2002). Anomalies of tropical averaged tropospheric temperature ($\langle \hat{T}' \rangle$) have been examined by Sun and Oort (1995) and Sun and Held (1996) in relation to humidity variations, noting the dominance of ENSO in the interannual variability. In addition to the use of $\langle \hat{T}' \rangle$ in global warming-related studies, widespread tropospheric temperature anomalies can potentially be important to teleconnections, both tropical and subtropical (Kiladis and Diaz 1989; Trenberth et al. 1998), because of the associated baroclinic pressure gradients. GCMs tend to reproduce $\langle \hat{T}' \rangle$ reasonably well (Soden 2000), even when important aspects of the hydrological cycle are less well simulated. Studies of the response to ENSO SST forcing (e.g. Lau 1985; Kiladis and Diaz 1989; Kumar and Hoerling 1998; Mechoso et al. 1987, etc.) have not yet addressed the mechanism of the tropospheric temperature response. Here, the relationship between tropical tropospheric temperature response and SST forcing is examined, focusing on the relationship between the local SST forcing and the very large scale temperature response and on what controls $\langle \hat{T}' \rangle$.

A distinct feature of the relationship between tropical tropospheric temperature and SST is the approximate linearity of temperature response to SST forcing. In Fig. 1, the tropical averaged (25 S-25 N) tropospheric (850-200 hPa) temperature anomalies are plotted against observed tropical SST anomalies (Reynolds and Smith 1994). Three temperature datasets are used. One is from the NCEP/NCAR (National Center for Environmental Prediction (NCEP)/National Center for Atmospheric Research) reanalysis data from 1982 to 1998 (Kalnay et al. 1996) and another is the satellite measurement (1982-1993) from the microwave sounding unit (MSU) associated with the vertical weighting functions of Channel 2-3 (Spencer and Christy 1992). The third is from a model simulation driven by observed SST anomalies from 1982-1998 (details in section 5). A similar scatter plot using tropical averaged temperature at 200 hPa is shown in Soden (2000) Fig. 5c. The approximate linearity demonstrated in Fig. 1 suggests that there ought to be some accessible dynamical explanation.

On the other hand, it is not obvious on physical grounds why the tropical averaged tropospheric temperature should have this apparent linearity with the tropical mean SST. The tropical response to SST certainly involves the complexities of moist convective dynamics. Anomalous precipitation response tends to depend not only on the SST anomaly but on the underlying climatological SST since precipitation tends to be organized in regions of the highest absolute SST. We thus wish to consider (1) why the approximate linearity should hold; (2) the question of the relative importance of different regions in contributing to $\langle \hat{T}' \rangle$: does the relatively small region which has warm SST anomalies added to high climatological SST dominate, or does the response depend on the whole region of warm SST anomalies? The latter question, first posed to us by I. Held, is examined from an observational standpoint in Sobel et al. (2002). They hypothesized that SST anomalies averaged over strongly precipitating regions (“rainy region SST”) are the dominant factor in setting $\langle \hat{T}' \rangle$ based on the argument that temperature profiles tend to be held to moist adiabats in deep convective regions and are less vertically constrained in non-precipitating regions. However, in Sobel et al’s results, tropical mean and rainy region SST anomalies both prove to be good predictors of $\langle \hat{T}' \rangle$ and it seems challenging to distinguish the two observationally. Here, these problems are approached from a modeling perspective: we design a set of experiments using SST anomalies of various shapes, magnitudes, and over different subregions of tropical Pacific Ocean and examine the tropical tropospheric temperature response to each SST distribution. The sensitivity of tropical tropospheric temperature to the shape, magnitude and location of SST forcing is thus explicitly quantified. The degree of nonlinearity in tropospheric temperature versus precipitation is also addressed. We focus on the seasonal averages of $\langle \hat{T}' \rangle$ and SST anomalies during peak El Niño seasons so the time lag in the atmospheric response is secondary. Analytical examination can thus use a steady state approximation.

The structure of the paper is as follows. Section 2 briefly describes the model physics and experiment design. Examples of model simulated temperature and precipitation anomalies during two El Niño events are presented in section 3. Section 4 describes the atmospheric response to subregions of warm SST anomalies based on 1997-1998 El Niño. Composites of tropical tropospheric temperature anomaly and precipitation anomaly from the regional SST anomaly experiments are presented in section 5. Section 6 examines the nonlinearity in the tropospheric temperature and precipitation responses using a set of experiments with specified SST anomalies in particular regions. To quantify the sensitivity of tropospheric

temperature to SST anomalies at different locations, sensitivity parameters are introduced in section 7 and the resulting similarity and difference of temperature–SST relations are noted for central Pacific and eastern Pacific regions. Section 8 attempts to explain the linearity of the temperature–SST relation analytically using the moist static energy balance. Conclusions and discussion are given in section 9.

2 Modeling approach

We use an intermediate complexity atmospheric circulation model—the quasi-equilibrium tropical circulation model (QTCM)—to address the mechanisms for tropospheric temperature anomalies associated with ENSO SST forcing. The QTCM is a primitive equation model that makes use of properties of a quasi-equilibrium moist convective closure to simplify vertical structures of atmospheric profile (Neelin and Zeng 2000; Zeng et al. 2000). The QTCM includes nonlinear advection, Betts-Miller moist convective adjustment, cloud-radiative interaction, and a simple interactive land model. It has been used for simulations involving tropical dynamics coupled with convection, land surface processes, and cloud-radiation feedback, etc. (e.g. Zeng and Neelin 2000; Lin et al. 2000; Chou et al. 2001; Su et al. 2001; and Su and Neelin 2002). In this study, the QTCM version 2.2 is used.

In addition to a simulation driven by observed SST from 1982-1998 (run OBS-SST), we conducted a number of simulations with specified SST distributions based on climatological SST plus subregions of the observed positive SST anomalies during two El Niño events. One is the 1997-1998 El Niño, and the other is the 1994-1995 El Niño. The former is one of the strongest warm events in the last century. The January-March (JFM) 1998 SST anomaly reached 3 C in the central and eastern Pacific (Fig. 2a). The latter is a relatively weak one. As shown in Fig. 3a, the average warming is less than 1 C and the maximum warm SST anomalies are concentrated near the dateline. For each SST distribution, ensemble means of ten simulations with slightly different initial conditions are constructed. Anomalies are defined by subtracting the ensemble means of ten control runs with climatological SST. The ten initial conditions are obtained from a 10-year simulation with seasonal SST. Because the variability between the elements of the ensemble are small compared to the signal of El Niño forced anomalies, some ensemble runs are done with only 3-5 elements. The responses in precipitation and tropospheric temperature anomalies are examined. Because the tropospheric temperature response extends throughout the tropics

even when SST anomaly forcing is localized, the behavior of the tropical average value is of interest.

Furthermore, we conducted simulations with arbitrary uniform SST anomalies added to climatological SST in particular regions. Three examples are shown for climatologically precipitating regions and one for a climatologically non-precipitating region. The response of tropical averaged tropospheric temperature to SST forcing is examined and compared to that of precipitation.

3 Examples of El Niño simulations

Run OBS-SST is conducted using observed SST from January 1982 to December 1998. Compared to observed tropospheric temperature and precipitation anomalies (Fig. 2b and 2c, Fig. 3b and 3c), the QTCM reproduces major features of the precipitation and tropospheric temperature response to El Niño SSTs for a very strong El Niño event, 1997-1998, and a relatively weak event, 1994-1995 (Fig. 4 and Fig. 5). For the JFM 1998 case (Fig. 4), the model captures the enhanced precipitation in the eastern-central Pacific and western Indian Ocean. To the north and southwest of the increased precipitation and in the western Pacific, negative precipitation anomalies were reproduced. The relative drought in northeast South America is weak in this run. This is likely caused by the model's overestimation of the effect of positive SST anomalies in the Atlantic Ocean, which counteracts the remote drying effect of warm SST anomalies in the Pacific Ocean. On the other hand, the simulated tropospheric temperature anomalies resemble the wide-spread warming of tropospheric temperature over the entire tropical band. Maximum temperature warming is in the eastern Pacific and Indian Ocean. Minimum warming is around the dateline. Around 30 N, there is a strong temperature gradient toward cold tropospheric temperature anomalies over parts of North America and the North Pacific, a remote response to El Niño (Lau and Nath 2001).

For the NDJ 1994-1995 case, the overall precipitation and tropospheric temperature anomalies are much weaker than the 1998 case. Maximum precipitation anomalies are around the dateline, near the maximum warming of SST (Fig. 3a). Warm tropospheric temperature anomalies spread over the tropics in both model results and NCEP reanalysis. The NCEP temperature anomaly toward mid-latitudes exhibits a wavy signal likely due to atmospheric variability which is not present in the QTCM simulation. Choosing the 25 S to 25 N band

for tropical averages is a reasonable compromise in avoiding such mid-latitude effects while capturing the broad tropical signal.

It is clear from both cases that the tropospheric temperature anomalies are wide-spread and relatively uniform over the whole tropical band. In contrast, the precipitation anomalies are localized. The strong positive precipitation anomalies occur near the warm SST forcing, while the tropospheric temperature anomalies have large spatial scales and a broad maximum that tends to be eastward of the maximum heating. This pattern is generally consistent with equatorial wave dynamics. The extension of warm anomalies away from the equator is related to the Rossby waves induced by convective heating associated with the warm SST anomalies while the Kelvin wave communicates the warming eastward. Because the wave dynamics is very effective at spreading the warming from a localized heat source, the entire tropical band displays a broad warming. The SST anomalies from other tropical oceans did impact the precipitation and temperature anomalies. For example, the warm SST anomalies in the Indian Ocean during the JFM 1998 force positive precipitation anomalies locally, as illustrated in Su et al. (2001). However, we will focus on the warm SST anomalies in the Pacific in later discussion because ENSO forcing is the leading effect. The fundamental dynamics of the response to SST forcing would presumably apply to all tropical ocean SSTs although details may vary from basin to basin.

4 Atmospheric response to subregions of El Niño SST

In order to examine the response of tropospheric temperature to El Niño SST anomalies of different shape and magnitude and over different regions, we performed experiments using subregions of the El Niño warm SST anomalies in the Pacific Ocean. Examples are shown for the 1998 JFM El Niño. The NDJ 1994-1995 results are similar to the 1998 case, although weaker in general. Figure 6 shows results for the experiment ENSOPAC, in which only positive SST anomalies within the heavy-outlined regions are included. The ENSOPAC outline is based on the 0.5 C contour of seasonal averaged SST anomalies for JFM 1998. Compared to Fig. 4 with full SST anomalies over the whole model domain, the ENSOPAC run produces similar patterns associated with the warm SST anomalies in the Pacific Ocean. The negative precipitation anomalies to the north and southwest of enhanced precipitation are simulated. The drought over northern South America is stronger than the OBS-SST run, suggesting that the Amazon drought is a remote response to the Pacific SST. The

teleconnections in the Indian Ocean and southeast of Africa display a weak drying effect. The negative precipitation anomalies in the western Pacific are absent in the ENSOPAC run. As described in Su et al. (2001), the negative precipitation anomalies in the western Pacific are primarily caused by local cold SST anomalies, which are not included in the ENSOPAC run. The positive precipitation anomaly is strongly localized to the region of the warm SST anomaly, although it is not proportional to it. In fact, the compensating descent (here seen as negative precipitation anomalies) begins within the boundary of the positive SST anomaly region. The main contributions to the compensating descent occur quite close to the positive precipitation anomaly (although weaker effects are seen in the far field). The tropospheric temperature anomaly, on the other hand, is spread over a much larger region, and is substantial over much of the tropical band, in accordance with observations (Wallace et al. 1998).

In subsequent experiments, we dissect the response to the 1997-98 El Niño positive SST anomaly by subdividing the region of warm SST anomalies into subregions and forcing the model with SST anomalies from each subregion in turn. Because the climatological SST in the tropics shows a strong zonal asymmetry, we first divide the ENSOPAC region into four subregions of similar size from west to east, as shown in Fig. 7. The sum of the precipitation and tropospheric temperature responses from the four subregions are shown in Fig. 7. Compared to the results from the total ENSOPAC run (Fig. 6), the sums of individual runs are very similar. However, negative precipitation anomalies are found within the positive SST anomaly region, at the boundaries of the subregions. This is because nonlinear advection effects come into play when strong gradients are artificially created in the subdivision processes. The nonlinear effect is more prominent in precipitation field than the tropospheric temperature field, as the temperature distribution more closely resembles the ENSOPAC experiment (Fig. 6b). The tropical averaged (25S-25N) tropospheric temperature anomaly is about 80% of that in the ENSOPAC run.

We also subdivide the ENSOPAC region into 8 and 16 subregions, and use the SST anomalies from each subregion to drive the QTCM. We note that there is a limit to how finely one can divide a given SST anomaly: if we subdivide the SST anomaly into relatively large subregions, then the sum of the responses is close to the response to the total. If smaller regions are used then the sum of the parts is smaller than the original due to nonlinear advectons. The tropical averaged tropospheric temperature is only 50% and 40% of the ENSOPAC run for the 8 and 16 subregions cases. However, the overall shape of temperature

response is still similar to the ENSOPAC run.

Figure 8 illustrates the results from one of the four subregions of SST anomaly runs. Although the positive precipitation anomalies are strongly localized to the warm SST anomalies, the tropospheric temperature anomalies display broad warming in the whole tropical band. The scope of the warming in both zonal and meridional directions is similar to that with the entire ENSOPAC SST anomaly. The maximum temperature warming is close to the SST anomaly region. Of course, the overall magnitude of tropospheric temperature warming is smaller than the ENSOPAC run. Figure 9 is another example of a subdivided SST anomaly experiment, in which only the positive SST anomalies within two degrees of the equator in the central Pacific are retained. Again, it is evident that the precipitation anomaly is highly localized within the area of positive SST anomaly. The tropospheric temperature anomaly, on the other hand, is spread over a wide region in the tropics. The distribution is similar to that of the entire SST anomaly in Fig. 6, although weaker (note the contour intervals differ). The temperature and associated wind anomalies are typical of wave response to localized heating source (Gill 1980). In Fig. 9, although the meridional extent of the positive SST anomalies is narrow, the tropospheric temperature warming still has a width characteristic of the radius of deformation, consistent with the effectiveness of wave dynamics in transporting the heating anomalies.

Differences in the patterns of temperature response may of course be seen for different SST forcing, especially in the subtropics. For present purposes, we focus on the similarity of the contributions to the large-scale average response.

5 Approximate linearity of tropospheric temperature - Model and Observations

As shown in Fig. 1, the observed tropical averaged tropospheric temperature anomalies appear more or less linear with tropical SST anomalies. The QTCM result from the OBS-SST run using observed SST anomalies from 1982-98 also shows a prominent linear relationship, whose slope is surprisingly close to those of the two independent observational datasets. All three slopes are approximately 1.4 C tropical averaged tropospheric temperature anomaly per degree C of tropical averaged SST anomaly. The model results have less scatter than the observed datasets due to reduced internal variability. Lagged analysis gives similar results. For instance, in the NCEP data, the regression slope is only about 10% larger at 1 month

lag than at 0 lag and drops for larger lags.

One might conjecture that linearity occurs in observations because the SST anomaly patterns tend to be similar. Does the approximate linearity exist for experiments with subregions of SST forcing? About 40 experiments were conducted with SST anomalies in subregions of different shapes, over different locations and of different areal extent, although all are based on the 1998 JFM SST anomaly in some way. The spatial average over the tropical band of tropospheric temperature from the QTCM is displayed as a function of SST forcing for the 40 experiments in Fig. 10a. The ordinate is the *spatial integral* of the SST anomaly. It can be seen that there is a remarkable degree of linearity of the response, despite the large range of regional size and spatial patterns sampled. Clearly, it matters how large the area of SST anomaly is, and regions other than the central Pacific do contribute.

For comparison, Fig. 10b displays the tropical averaged precipitation anomalies versus SST forcing for the same set of experiments. It is clear that the tropical averaged precipitation anomaly bears no simple relation to SST forcing, nor does it to the tropospheric temperature anomaly. Examples of the spatial distribution of precipitation anomalies are shown in side panels. While the spatial patterns are qualitatively similar, the average is set by the sum of positive anomalies local to the SST forcing versus weaker negative anomalies that may occur over a larger area. The near-cancelation can produce either sign in the tropical average. Overall, the different behavior of the tropical averaged precipitation and temperature illustrates an important feature in the tropical atmospheric response to SST forcing. Convection plays an active role in transporting the boundary forcing upward through the entire troposphere, tending to constrain the tropospheric temperature. However, the amount of *convective heating* is governed by balances with various cooling mechanisms which have a more complex dependence (Su and Neelin 2002).

In terms of spatial distribution of anomalies, the difference noted in the previous section between the tropospheric temperature and precipitation responses holds for all the experiments of subregion SST forcing. The direct, positive response of precipitation to a positive SST anomaly is much more local and tends to be surrounded by negative anomalies. The tropical averaged precipitation is thus a sum over large positive and negative values, leaving room for nonlinearity to complicate the response. The temperature anomaly, on the other hand, tends to have very large scales set by tropical wave dynamics.

We note that the linearity applies only to large-scale aspects of the tropospheric temperature pattern. Considering the response to SST anomaly forcings that have small spatial

area (the lower end of the scatter plot in Fig. 10a), nonlinearity does play a role as those points fall below the linear fit. The precipitation response in this model has the same strong nonlinearity at the edges of convection zones as seen in observations.

6 Nonlinearity of temperature and precipitation anomalies

To quantify the extent of nonlinearity in tropospheric temperature and precipitation responses, we conducted experiments with SST anomalies of -5 C up to 5 C in specific regions. For such experiments, we choose four subregions, shown in Fig. 11 and Fig. 12. In Fig. 11, subregion 1 is climatologically precipitating, while regions 3 and 4 are mixtures of precipitating and low-precipitation regions. The shapes of subregions are the same as the ones used in the four subregions of the ENSOPAC run. In Fig. 12, the target area is a climatologically non-precipitating region during September to November.

For all four regions, the modeled tropical averaged tropospheric temperature response (Fig. 11a and 12a) falls along a smooth nonlinear curve but the departure from linearity is modest. The linear fits using experiments with small SST anomalies (-0.5 C to 0.5 C) are plotted for comparison. The slopes of these linear fits correspond to a model linearized about climatology. We use this slope α of tropical averaged tropospheric temperature response versus tropical averaged SST anomalies as a standard measure of sensitivity. Their values are 2.40, 1.75, 1.44 for regions 1, 3, 4, respectively, and 0.53 for the non-precipitating region. Linear fits using SST anomalies within the observed SST anomaly range (marked in thicker grey within bars in Fig. 11a and 12a) are very close, with corresponding slopes of 2.38, 1.80, 1.53, 0.62 for the four regions, respectively. The small SST anomaly linear fits capture over 95% of the actual model response within the observed SST anomaly range. Even for SST anomaly as large as 3 C, which rarely occurs in nature, the departure from linearity is only 15% in the central Pacific and smaller for other regions.

On the other hand, local precipitation response shows dramatic nonlinearity over the climatologically non-precipitating region (Fig. 12b), compared to the temperature response. The regional-averaged precipitation anomalies are virtually zero until the added SST anomalies are more than 2 C and increase rapidly for large SST anomalies. A linear fit to the precipitation anomalies would fail badly in this region. Local precipitation response over the climatologically precipitating regions (Fig. 11b) shows weaker nonlinearity over the range of

SST anomaly tested. The nonlinearity is strongest for large negative SST anomalies as total precipitation becomes small. For region 4, for an SST anomaly of -3 C, the error of linear fit is about 50%.

From west to east in the Pacific Ocean, the slope α gradually decreases from 2.40 to 1.44 for the subregions that include some precipitation. The slope over the climatologically non-precipitating region is even smaller (0.53). The slope for the observed tropospheric temperature response to SST forcing ($1.4CC^{-1}$) lies midway in this range, consistent with observed SST sampling a variety of these regions.

We note the caveat that the non-precipitating region in Fig. 12 is off the equator and thus dynamical factors may also impact the sensitivity. The projection of the effect of the SST anomalies onto the atmospheric equatorial Kelvin wave will tend to be smaller than for anomalies on the equator. However, this tends to affect the spatial broadness of temperature anomalies more than the average temperature response because the latter is approximately set by the balance between radiative cooling and surface forcing.

7 Sensitivity Parameters For Subregions

It has been argued (Sobel et al. 2002) that the tropical tropospheric temperature anomalies should be dominated by SST anomalies over regions of high climatological SST. The slightly higher slopes of temperature response to SST forcing in Fig. 11a than that in Fig. 12a suggest there may indeed be an SST dependency of the sensitivity of tropical tropospheric temperature response to SST forcing. We thus introduce two measures of sensitivity, shown in Fig. 13 using the four subregion experiments of the ENSOPAC run for the JFM 1998 and NDJ 1994-1995 El Niños as examples. The first is a sensitivity parameter giving the response per unit forcing, where the forcing is defined as the spatial integral of the SST anomaly over the region. Note this is not the same as the linear sensitivity α since it includes finite amplitude effects. The second is the contribution of each region as a fraction of the tropical-average tropospheric temperature anomaly in the full ENSOPAC SST anomaly experiment.

For the JFM 1998 case, the sensitivity is noticeably larger in the central Pacific region where absolute SST is higher, but it does not become small in the other regions. Since the middle two of the four regions have larger SST anomalies, these actually contribute more to the JFM 1998 tropospheric temperature anomaly in percentage contribution than the region near the dateline.

The NDJ 1994-1995 El Niño displays similar sensitivity parameters even though this event is much weaker than the 1998 El Niño (Fig. 13b). In this case, the highest percentage contribution came from the subregion in the central Pacific where the warmest SST anomalies were concentrated. However, the contribution from the eastern-most subregion is not negligible.

8 Analytical Explanation

8.1 Consequence of tropical averaged flux balance

The linearity of tropospheric temperature with SST forcing suggests an accessible dynamical explanation. We use the moist static energy equation to illustrate this analytically.

The vertically-integrated MSE perturbation equation in the QTCM takes a simple form

$$\widehat{\mathcal{D}}_T T' + \widehat{\mathcal{D}}_q q' + (M_1 \nabla \cdot \mathbf{v}_1)' = (g/p_T)(F_{\text{rad}}' + H' + E') \quad (8.1)$$

We note

$$\widehat{T}' = \widehat{a}_1 T_1', \widehat{q}' = \widehat{b}_1 q_1' \quad (8.2)$$

where T_1 and q_1 are the projection coefficients of atmospheric temperature and moisture onto the first retained baroclinic mode in the model (Neelin and Zeng 2000). The parameters \widehat{a}_1 and \widehat{b}_1 are the vertical integrals of temperature and moisture profiles. The first two terms $\widehat{\mathcal{D}}_T T'$ and $\widehat{\mathcal{D}}_q q'$ denote the perturbations of horizontal advection and diffusion of temperature and moisture. The vertical advection of MSE is taken as the horizontal divergence anomaly $(\nabla \cdot \mathbf{v}_1)'$ weighted by the “gross moist stability” parameter M_1 . The gross moist stability combines the effect of adiabatic cooling and convective heating over convective regions (see Neelin and Zeng 2000). These terms on the l.h.s. represent the perturbation transport of MSE and the terms on the r.h.s. correspond to column-averaged forcing due to the surface and radiative flux anomalies. The total radiative heating rate is denoted as F_{rad} . The surface sensible and latent heat fluxes are H and E , respectively, and $p_T = p_{rs} - p_{rt}$ is the constant reference pressure depth of the troposphere and the $()'$ denotes the perturbation from climatological state.

Because of the broadness of tropical tropospheric temperature anomalies, the tropical averages of each quantity are of interest. When averaged over the whole tropical band (e.g., 25 S - 25 N), the sum of the transport terms on the left hand side of the equation is small compared to the dominant balance on the right hand side. For example, the tropical averaged

perturbation transport of MSE in the ENSOPAC run is 0.07 Wm^{-2} , whereas the averaged E' and F_{rad}' are 1.1 Wm^{-2} and 1.5 Wm^{-2} , respectively. Even the averaged H' is around 0.6 Wm^{-2} . (In the OBS-SST run, the total perturbation transport is secondary but less negligible. It more or less tracks the evolution of evaporation anomalies so could be treated as a small reduction of forcing related to T'_s . This provides little additional insight so is omitted for simplicity.) The smallness of area averaged transports yields a simple energy balance between radiative fluxes and surface heat fluxes, to a first-order approximation,

$$\langle F_{\text{rad}}' + H' + E' \rangle \approx 0. \quad (8.3)$$

Here we use $\langle \rangle$ to denote the averages over the whole tropical band.

The radiative heating rate is approximately a linear function of temperature, moisture, surface temperature and cloud fractions. In the model,

$$F_{\text{rad}}' \approx -\epsilon_T T_1' - \epsilon_q q_1' + \epsilon_{T_s} T_s' + (CRF)', \quad (8.4)$$

where ϵ_T , ϵ_q , and ϵ_{T_s} are the coefficients for radiative heating rate in the air column per unit change in the projection coefficients of temperature and moisture, and surface temperature change. The values of ϵ_T , ϵ_q , and ϵ_{T_s} are 2.89, 1.11 and 5.98, respectively (the sign convention for ϵ_T and ϵ_q differs from Neelin and Zeng 2000). $(CRF)'$ represents the radiative heating rate of the atmospheric column due to cloud fraction change. As described in Su and Neelin (2002) and Appendix A, the cloud radiative forcing is approximately proportional to the precipitation anomalies with a cloud radiative feedback parameter C (see Appendix A).

Since tropical averaged precipitation anomalies P' approximately balance evaporation anomalies E' , the cloud-radiative feedback term is absorbed in the flux balance with modification on the weighting of evaporation term. Thus we have

$$\langle -\epsilon_T T_1' - \epsilon_q q_1' + \epsilon_{T_s} T_s' + H' + (1 + C)E' \rangle \approx 0 \quad (8.5)$$

Hence, the role of clouds can be regarded as an increase in the column-averaged forcing (warming during El Niño, and cooling for La Niña). Its magnitude is about 12% of the evaporation anomaly.

Using the conventional bulk aerodynamic formula for surface heat fluxes, and including only the contribution to surface heat flux anomalies by the temperature and moisture anomalies, we obtain a simple relation for tropical tropospheric temperature and moisture

anomalies with SST forcing

$$\begin{aligned} \epsilon_T \langle T_1' \rangle + \epsilon_q \langle q_1' \rangle + \langle \epsilon_H \bar{V}_s a_{1s} T_1' \rangle + \langle (1+C) \epsilon_H \bar{V}_s b_{1s} q_1' \rangle \approx \\ \epsilon_{T_s} \langle T_s' \rangle + \langle \epsilon_H \bar{V}_s T_s' \rangle + \langle (1+C) \epsilon_H \bar{V}_s \gamma T_s' \rangle \end{aligned} \quad (8.6)$$

where $\epsilon_H = \rho_a C_H \approx 1.09$, The climatological surface wind speed is denoted as \bar{V}_s and $\gamma = \left(\frac{dq_{\text{sat}}}{dT} \right)_{T_s}$. We note that the contribution of wind anomalies to surface heat fluxes is neglected, as it is smaller than the terms retained (about 30% of E' due to $\langle \epsilon_H \bar{V}_s T_s' \rangle$ and of opposite sign in the positive SST forcing regions).

Both observations and model experiments show that $\langle q_1' \rangle$ bears a linear relationship with both $\langle T_1' \rangle$ and $\langle T_s' \rangle$, as discussed in section 8.2. With this $\langle q_1' \rangle$ dependence specified, (8.6) gives the approximate linear relationship of tropical averaged tropospheric temperature and SST anomalies. The dynamic processes involved are as follows: during El Niño, warm SST anomalies induce stronger than normal evaporation, sensible heat flux and the radiative heating from the surface. These result in higher than normal boundary layer MSE and thus stronger convection. Increased convective heating warms the troposphere and wave dynamics spread out the warming to remote regions. The warmer and moister surface air tend to counteract the increase of surface heat fluxes. And the radiative cooling over a large area associated with positive atmospheric temperature and moisture anomalies balances the surface forcing due to the regional warm SST anomaly. Cloud-radiative feedback effectively increases the surface forcing as larger than normal cloud fraction reduces outgoing longwave radiation and warms the atmospheric column. Vice versa for La Niña events. Hence, the spatial pattern of tropospheric temperature anomalies is wide-spread over the whole tropical band. The linearity of tropical averaged tropospheric temperature anomalies to SST forcing is a direct consequence of approximate flux balance within the atmospheric column. A key factor is the nonlinear transport terms are small when averaged over a large horizontal area. For SST anomaly forcing concentrated in a climatologically non-precipitating region, increased evaporation due to warm SST anomaly changes moisture advection and convergence from the region and increases precipitation outside the forcing region. Again, wave dynamics is effective in transporting the warming over the entire tropics and radiative cooling and increased surface air temperature and moisture balance increased surface heat fluxes due to SST warming.

From (8.6), we notice that the precipitation anomaly or convective heating anomaly does not appear. This is fortunate, given that in Fig. 10b it was shown that *tropical averaged*

precipitation anomaly is not related to SST or tropospheric temperature anomalies in a simple manner. This reflects an important aspect of the relation between atmosphere response and SST forcing: convection acts as a mediator to raise the tropospheric temperature to a value set by SST. However, the amount of convective heating required to do this depends on what mechanisms oppose it (Su and Neelin 2002). The tropospheric temperature response is simpler than the convective heating response and is addressed here, via (8.6).

8.2 Regional difference in slope α of $\langle T' \rangle$ versus $\langle T_s' \rangle$

The equation (8.6) is given in terms of tropical averages. Why does there exist regional difference in the slope α of $\langle T' \rangle$ versus $\langle T_s' \rangle$ as illustrated in Fig. 11 and Fig. 12? This is because the SST forcing is localized in experiments where it is specified only in certain regions. The regional climatology enters through several factors. For instance, because $T_s' = 0$ outside the experiment region, $\langle \bar{V}_s \gamma T_s' \rangle \approx (\bar{V}_s \gamma)_{region} \langle T_s' \rangle$ and $\langle \bar{V}_s T_s' \rangle \approx (\bar{V}_s)_{region} \langle T_s' \rangle$ where $(\bar{V}_s \gamma)_{region}$ and $(\bar{V}_s)_{region}$ use values of wind speed and γ , that are typical of the experiment region. The value of γ increases with climatological SST and thus tends to yield higher sensitivity in tropospheric temperature response when anomalies occur in warm SST regions.

Another more sensitive factor in determining the slope α is how $\langle q_1' \rangle$ is related to $\langle T_1' \rangle$ or $\langle T_s' \rangle$. As mentioned before, $\langle q_1' \rangle$ bears a linear relationship with both $\langle T_1' \rangle$ and $\langle T_s' \rangle$. However, the exact dependence of $\langle q_1' \rangle$ on $\langle T_1' \rangle$ or $\langle T_s' \rangle$ varies significantly between experiments with SST forcing in precipitating regions and non-precipitating regions. This indicates that different dynamics govern the response of moisture to SST forcing over different regions. To diagnose the regional differences in α , we separate the response of moisture in precipitating and non-precipitating regions and obtain an approximate linearized relation based on the dominant thermodynamical balance in each region. This results in the following approximate relation,

$$\langle q_1' \rangle = n A_P \langle T_1' \rangle_P + m A_{NP} \langle T_s' \rangle_{NP}, \quad (8.7)$$

where A_P and A_{NP} are the fractional area of precipitating and non-precipitating regions, respectively, n and m are proportionality constants that apply in each region. In precipitating regions, the moisture anomaly is related to tropospheric temperature anomaly by moist convective constraints, which yields n . We find

$$\langle T_1' \rangle_P \approx \langle T_1' \rangle \quad (8.8)$$

holds reasonably well because of the broadness of temperature anomalies. In non-precipitating regions, the moisture anomaly is related to the local SST anomaly through a balance of evaporation, advection, dissipation, and divergence terms, which results in m . The derivation of n and m are given in Appendix B. The values of n and m estimated from these derivations are 0.9 and 2.1. Empirical linear fits to the model results for $\langle q'_1 \rangle$ in the respective regions give $n \approx 0.9$ and $m \approx 2.7$. The reason that the derived m value is only qualitative is discussed in the Appendix B. The fitted value is used for α calculations below.

Since m gives the relation to SST anomalies in non-precipitating regions $\langle T'_s \rangle_{NP}$, we write

$$A_{NP} \langle T'_s \rangle_{NP} = \sigma \langle T'_s \rangle, \quad (8.9)$$

where the ‘‘SST anomaly shape factor’’ σ represents the percentage of SST anomalies that are over non-precipitating regions. This σ is a purely diagnostic factor and varies with different SST distributions. If $\langle T'_s \rangle$ lies entirely in precipitating regions, $\sigma = 0$, while $\sigma = 1$ for $\langle T'_s \rangle$ in non-precipitating regions. In the model run using observed SST from 1982 to 1998, the 17-year averaged σ is approximately 0.25 (for years with $\langle T'_s \rangle$ greater 0.05 C).

Finally, the slope α of tropical-averaged tropospheric temperature anomalies versus tropical mean SST anomalies can be obtained as

$$\alpha [\epsilon_T + \epsilon_H (\bar{V}_s)_{trop} a_{1s} + n A_{NP} \epsilon_q + (1 + C) \epsilon_H (\bar{V}_s)_{trop} b_{1s}] \approx \hat{a}_1 [\epsilon_{T_s} + \epsilon_H (\bar{V}_s)_{region} + (1 + C) \epsilon_H (\bar{V}_s)_{region} \gamma - m \sigma [\epsilon_q + (1 + C) \epsilon_H (\bar{V}_s)_{region} b_{1s}]] \quad (8.10)$$

Table 1 shows the typical parameter values and resulting slopes for a number of cases. In the first five cases, the parameters input to (8.10) are chosen to mimic the QTCM experiments. The first four correspond to our model experiments for the small SST anomaly experiments in precipitating regions and a non-precipitating region. The fifth one (OBS-SST) is associated with the 17 year run with observed SST from 1982 to 1998. The parameters are approximately tropical mean values. The last three are examples based on the OBS-SST case but varying each parameter to see the effects of climatological SST, wind speed, and the SST anomaly shape factor, σ , respectively. The analytical results are generally consistent with the linear fits of model simulations. The highest value of α is somewhat less than that obtained in the QTCM. For the variations on the OBS-SST case, a 2 degree difference in climatological SST increases α slightly (about 8%). The change to a 100% precipitating domain causes a 20% increase. The wind speed change gives the highest sensitivity in the observed case. With an average of 2 m s^{-1} increase of wind speed, the temperature slope is

raised by 36%. Note that these three cases are based on the observed value of σ , which is dominated by precipitating regions. The difference in α from partially-precipitating to all-precipitating is relatively small, whereas the regional SST anomaly experiments show that the transition from precipitating to non-precipitating regions yields substantial difference in the slope of tropical tropospheric temperature response to SST forcing.

In the above analysis, surface heat flux and radiative flux anomalies outside the anomalous SST forcing region do come into play when a large horizontal area is considered. The tropical averaged tropospheric temperature is determined non-locally through wave dynamics by tropical mean SST forcing. Linearity dominates the relationship between tropospheric temperature and SST forcing, although regional climatology and different dynamics of moisture response over precipitating and non-precipitating regions add complexity to the $\langle \hat{T}' \rangle$ to $\langle T'_s \rangle$ relationship. Note that a variety of weighted averages that affect fluxes have been approximated here. The separation of precipitating and non-precipitating regions is one example of such weighting. The weighting by wind speed is another factor that is potentially equally important.

9 Conclusions and discussion

Observations of tropically averaged tropospheric temperature anomalies exhibit an approximately linear relationship with tropical mean SST anomalies, which are substantially associated with ENSO variability. The intermediate complexity atmospheric model forced with observed SST data reproduces this linear relationship and thus can be used to dissect it. A large number of experiments were conducted with SST anomalies of different shape, areal extent and magnitude in tropical Pacific regions of different climatological SST. The approximate linearity in the tropospheric temperature response to SST forcing was found to hold fairly generally for this set of forcings. The tropospheric temperature response is approximately linear with the spatial integral of SST forcing, so the areal extent and magnitude of SST anomalies both affect the temperature response. To a first-order approximation, the horizontal distribution of tropospheric anomalies tends to be similar regardless of where the SST forcing is located. The spatial pattern generally resembles the traditional wave response to a localized heat source, although with large longitudinal extent compared to heavily damped simple models. Because the spatial extent of the temperature response is large even when the SST forcing is highly localized, the tropical mean tropospheric temperature

response anomaly $\langle \hat{T}' \rangle$ is highly relevant as a measure of the dynamical response, in addition to being of interest in global warming related studies.

Although linearity dominates in the tropical tropospheric temperature response to SST forcing, nonlinearity is inevitable due to the involvement of nonlinear advection, moist convection and cloud-radiation feedback, etc. Experiments were designed using successively smaller SST anomalies in various subregions to quantify the extent of nonlinearity in the tropical tropospheric temperature and precipitation responses to SST forcing. We found that nonlinearity accounts for only 5% of total temperature response for SST anomalies within the observed range. Even for an SST anomaly as large as 3 C, the departure from linearity is merely 15% in the central Pacific and smaller for regions further east. This holds for regions of modest areal extent (on the order of 25 degrees by 20 degrees). For smaller regions, where small areal extent allows greater impact of the SST gradient at the edges of subregions, nonlinearity becomes more significant. For more widespread or smaller amplitude anomalies, the departure of the nonlinear solution from a linear fit is smaller. The appearance of linearity in the response to the time history of observed anomalies likely results from a combination of the broad spatial scales of typical anomalies and the infrequency of events as large as the 1997-1998 El Niño.

Another measure of nonlinearity is the extent to which the sum of the responses to subregions of an SST anomaly approximates the response to the full SST anomaly. For the modest sized regions (four subregions within the El Niño SST anomaly region), the spatial pattern of tropospheric temperature for the sum of the responses closely resembles the full response, although the amplitude is slightly smaller. Even for a large event such as the 1997-98 El Niño, the sum of $\langle \hat{T}' \rangle$ for four regions gives about 80% of the full response, consistent with the degree of nonlinearity estimated by increasing SST in an individual subregion. Thus one can use the response to individual subregions (as a fraction of the response to the sum of subregions) to characterize the sensitivity for regions with higher or lower climatological SST. This is subject to the caveat that the subregions should not be too small due to increasing nonlinearity.

The sensitivity of tropospheric temperature response to El Niño SST forcing tends to decrease from west to east in the Pacific. This holds for both small amplitude estimates of sensitivity or finite amplitude estimates using subregions of observed anomalies. The sensitivity of $\langle \hat{T}' \rangle$ is larger for SST anomalies in regions of high climatological SST, as expected. However, SST anomalies in climatologically colder regions are far from negligible.

For the example of the 1997-1998 El Niño, the contribution of the anomalies in eastern Pacific region to $\langle \hat{T}' \rangle$ is actually larger than the contribution of anomalies near the date line, despite lower climatological SST. This is simply because the anomalies are larger, even though the sensitivity is lower.

Precipitation anomalies in these experiments tend to exhibit stronger nonlinearity than the tropospheric temperature. For instance, nonlinear effects at the boundaries of subregions are visible when summing subregions. The onset of precipitation in a sequence of experiments increasing SST in a climatologically non-precipitating region is clearly poorly fit by a linear approximation, although temperature increase in this same sequence of experiments has substantially smaller departures from linearity. The tropical averaged precipitation anomalies have no simple relation to SST forcing, nor to the tropospheric temperature anomalies. This may be relevant to the greater ease with which GCMs reproduce tropical-averaged temperature than tropical-averaged precipitation, noted by Soden (2000). The region of strongest precipitation tends to be localized to the region of SST anomalies if they occur in a climatologically precipitating region, with weaker negative precipitation anomalies occurring by teleconnections in surrounding regions. If the anomalous SST forcing occurs in a non-precipitating region, positive precipitation anomalies tend to occur at the margins of the neighboring precipitating region, while weak negative precipitation occurs over a broader region. While *convection* is important in communicating the boundary forcing upward to constrain the tropospheric temperature, the amount of *convective heating* is subject to complex balance of various cooling mechanisms (Su and Neelin 2002).

Define α to be the slope of the $\langle \hat{T}' \rangle$ dependence on SST, where the SST is expressed as a tropical average even if it is only a local SST anomaly. The linear fit slope for the observed $\langle \hat{T}' \rangle$ to $\langle T_s \rangle'$ relation is about 1.4 for MSU and NCEP data and for the QTCM simulation. For the subregion SST anomaly experiments, α varies from about 2.4 in the central Pacific to as little as 0.5 in the southeastern tropical Pacific in the dry season when the region is strictly non-precipitating. We note that the exact numbers of sensitivity parameters may be model-dependent, although the general trend should hold as our results.

An analytic approach is used to diagnose the physical mechanisms contributing to this slope. When the moist static energy equation is averaged over a large horizontal area, such as the tropical domain, the transport terms are negligible since the fluxes out the boundaries of the domain are relatively small. This yields a simple energy balance between the surface and top-of-atmosphere heat and radiative fluxes. The tropical average heat fluxes have only

a weakly nonlinear dependence on temperature. The strong nonlinearities that occur locally tend to be associated with the transport terms. Thus the approximate linearity of the $\langle \hat{T}' \rangle$ response is due to two factors: the large-area average removing the transport terms; and the weak nonlinearity of the flux dependence on temperature.

Linearizing the flux terms, the problem is not closed for the relation of moisture to temperature variables, but estimates of this dependence from the nonlinear model can be used in the spirit of diagnosing the mechanisms. In precipitating regions, moisture is fairly closely tied to tropospheric temperature by convective constraints. In non-precipitating regions, the moisture anomalies are poorly related to tropospheric temperature anomalies but are related to SST anomalies by a complex balance involving evaporation, advection and divergence terms. The result is that moisture increases cause evaporation to increase less rapidly with SST in non-precipitating regions than in precipitating regions. Water evaporated in the non-precipitating region does contribute to tropical warming by precipitating elsewhere, but the net warming that must be balanced by longwave radiation from the troposphere is smaller in the tropical average than for an SST anomaly in a precipitating region.

The resulting estimates for α include several weighted averages of SST anomalies that must be approximated, including factors due to climatological SST, wind speed and whether or not the region is strongly precipitating. These weighting factors yield the dependence of α on region. Climatological SST per se yields only a modest difference in α between warm and cold tropical regions. Wind speed has a fairly strong effect on slope but tends to oppose the direct effect of SST since cold SST regions often have stronger climatological wind which would yield larger slopes. A substantial contribution to regional variation in α comes from the different reaction of moisture in precipitating and non-precipitating regions. However, the observed slope is not as strongly affected by changes in the fraction of non-precipitating regions as it would be by changes in wind speed.

Acknowledgments. This work was supported under National Science Foundation Grant ATM-0082529, National Oceanographic and Atmospheric Administration Grant NA16-GP2003 and National Aeronautics and Space Administration Grant NA-GS-9358. This is UCLA IGPP contribution 5756. The authors thank I. Held for suggesting the subject to us and A. H. Sobel for discussions and manuscripts of related work.

Appendix

A Approximate tropical averaged flux balance

Using the tropical averaged MSE equation (8.1) and neglecting the perturbation transport terms, we obtain an approximate flux balance averaged over the tropics(8.3).

In (8.3), the radiative heating rate is approximately a linear function of temperature, moisture, surface temperature and cloud fractions. The cloud radiative heating rate is parameterized approximately proportional to the precipitation anomalies

$$(CRF)' \approx CP', \quad (\text{A.11})$$

where C is a cloud radiative feedback parameter. When computed from the QTCM cloud radiative parameters, $C \approx 0.12$ in the version 2.2 of the QTCM. This value includes both longwave and shortwave radiative effects, but since it is defined for the difference between the top-of-atmosphere and surface radiative fluxes, it is dominated by longwave effects.

Applying the moisture equation, the precipitation anomalies consist of contributions from anomalies of moisture convergence, moisture advection and evaporation. When averaged over the tropics, the first two terms are close to zero. Thus,

$$\langle P' \rangle \approx \langle E' \rangle. \quad (\text{A.12})$$

Substituting (8.4), (A.11) and (A.12) into (8.3), we have

$$\langle -\epsilon_T T_1' - \epsilon_q q_1' + \epsilon_{T_s} T_s' + H' + (1 + C)E' \rangle \approx 0. \quad (\text{A.13})$$

The surface heat fluxes are parameterized using bulk aerodynamic formula. Including only the contribution to surface heat flux anomalies from the temperature and moisture anomalies, the surface heat flux anomalies are approximated as

$$H' \approx \rho_a C_H \bar{V}_s (T_s' - a_{1s} T_1') \quad (\text{A.14})$$

and

$$E' \approx \rho_a C_H \bar{V}_s (q_{\text{sat}}(T_s)' - b_{1s} q_1'), \quad (\text{A.15})$$

where \bar{V}_s denotes the climatological surface wind speed.

The contribution of wind anomalies to surface sensible heat flux and evaporation anomalies is neglected here, as discussed in the text. Within the normal range of surface temperature variation, the saturation surface moisture q_{sat} is nearly linear with surface temperature change

$$q_{\text{sat}}(T_s)' \approx \gamma T_s', \quad (\text{A.16})$$

where

$$\gamma = \left(\frac{dq_{\text{sat}}}{dT} \right)_{T_s}. \quad (\text{A.17})$$

Using the above approximations, we obtain a simple relation for tropical tropospheric temperature and moisture anomalies with SST forcing (8.6).

B Diagnosis of tropical averaged tropospheric moisture anomalies in relation to temperature and SST anomalies

Considering the different moist dynamics in precipitating and non-precipitating regions, one can partition the tropical averaged moisture anomalies into two parts:

$$\langle q_1' \rangle = \langle q_1' \rangle_P A_P + \langle q_1' \rangle_{NP} A_{NP}, \quad (\text{B.18})$$

where $\langle q_1' \rangle_P$ and $\langle q_1' \rangle_{NP}$ represent the average moisture anomalies for precipitating and non-precipitating regions, respectively, and A_P and A_{NP} denote the fractional area of each region, with $A_P + A_{NP} = 1$.

For precipitating regions, the atmospheric profiles of temperature and moisture are adjusted by convection under quasi-equilibrium convective closure (Neelin and Zeng 2000). The moisture anomaly tends to approach its quasi-equilibrium value $\langle (q_1^{QE})' \rangle$.

$$\langle q_1' \rangle_P \approx \langle (q_1^{QE})' \rangle \quad (\text{B.19})$$

Numerically linearizing the nonlinear QTCM convective scheme gives

$$\langle (q_1^{QE})' \rangle \approx n \langle T_1' \rangle_P \quad (\text{B.20})$$

with $n \approx 0.9$ (analytical linearization for n is possible but adds little insight). Using $\langle T_1' \rangle_P \approx \langle T_1' \rangle$ because of the broadness of temperature anomalies, this yields a quasi-linear relation between $\langle q_1' \rangle_P$ and $\langle T_1' \rangle$

$$\langle q_1' \rangle_P \approx n \langle T_1' \rangle. \quad (\text{B.21})$$

For non-precipitating regions, moisture anomalies are determined by dynamics without convection. Using the temperature and moisture equations of the QTCM (ignoring transport terms in temperature equation because of weak temperature gradient in the tropics (Sobel and Bretherton 2000)), we have

$$(M_{s1}\nabla \cdot \mathbf{v}_1)' = (g/p_T) (-\epsilon_T T_1' - \epsilon_q q_1' + \epsilon_{T_s} T_s' + H') \quad (\text{B.22})$$

$$(\widehat{\mathbf{v}} \cdot \nabla q)' - \widehat{b}_1 K_H \nabla^2 q_1' - (M_{q1} \nabla \cdot \mathbf{v}_1)' = (g/p_T) E' \quad (\text{B.23})$$

where

$$(\widehat{\mathbf{v}} \cdot \nabla q)' \approx \widehat{b}_1 \overline{\mathbf{v}}_q \cdot \nabla q_1' + \widehat{b}_1 \mathbf{v}_q' \cdot \nabla \overline{q}_1, \quad (\text{B.24})$$

with $\mathbf{v}_q = (\widehat{b}_1 \widehat{\mathbf{v}}) \widehat{b}_1^{-1}$, a vertical average of wind weighted by moisture structure (see Neelin and Zeng 2000 for details). Because \mathbf{v}_q' is not easily related to T_s' or T_1' it must be neglected, with consequence below. Advection of anomalous moisture by climatological winds is approximated as $\widehat{b}_1 \overline{\mathbf{v}}_q q_1' / L_{NP}$, with L_{NP} the typical length scale of q' associated with the non-precipitating region experiments, and $\overline{\mathbf{v}}_q$ a typical magnitude of $\overline{\mathbf{v}}_q$. Similarly, the horizontal diffusion anomalies are approximately as $\widehat{b}_1 K_H q_1' / (L_{NP})^2$. Neglecting sensible heat flux anomalies H' and radiative flux anomalies due to temperature and moisture anomalies and with less justification neglecting \mathbf{v}' effects on E' , we have

$$\overline{M_{s1}} (\nabla \cdot \mathbf{v}_1)' \approx (g/p_T) \epsilon_{T_s} T_s' \quad (\text{B.25})$$

$$\begin{aligned} \widehat{b}_1 \overline{\mathbf{v}}_q q_1' / L_{NP} + \widehat{b}_1 K_H q_1' / L_{NP}^2 - \overline{M_{q1}} (\nabla \cdot \mathbf{v}_1)' - M_{qp1} q_1' (\overline{\nabla \cdot \mathbf{v}_1}) \approx \\ (g/p_T) (\epsilon_H \mathbf{V}_s^c) (\gamma T_s' - b_{1s} q_1') \end{aligned} \quad (\text{B.26})$$

Then we arrive at a relation between $\langle q_1' \rangle_{NP}$ and $\langle T_s' \rangle_{NP}$.

$$\langle q_1' \rangle_{NP} \approx \frac{\epsilon_H \overline{\mathbf{V}}_s \gamma + (\overline{M_{q1}} / \overline{M_{s1}}) \epsilon_{T_s}}{(p_T/g) (\widehat{b}_1 \overline{\mathbf{v}}_q / L_{NP} + \widehat{b}_1 K_H / L_{NP}^2 - M_{qp1} \overline{(\nabla \cdot \mathbf{v}_1)}) + \epsilon_H \overline{\mathbf{V}}_s b_{1s}} \langle T_s' \rangle_{NP} \quad (\text{B.27})$$

Applying the averaged values from the model experiment for the parameters in (B.27) ($\epsilon_H = 1.1$, $\overline{\mathbf{V}}_s = 7.5$, $\gamma = 2.5$, $\overline{M_{q1}} = 3.0$, $\overline{M_{s1}} = 3.5$, $\epsilon_{T_s} = 5.98$, $\overline{\mathbf{v}}_q = 7.5$, $L_{NP} = 5 \times 10^6$, $K_H = 9.0 \times 10^5$, $M_{qp1} = 0.05$, $\overline{(\nabla \cdot \mathbf{v}_1)} = 10^{-6}$, $b_{1s} = 1$, $\widehat{b}_1 = 0.33$, $p_T/g = 8 \times 10^6$) yields

$$\langle q_1' \rangle_{NP} \approx m \langle T_s' \rangle_{NP} \quad (\text{B.28})$$

with $m \approx 2.1$. A linear fit of $\langle q_1' \rangle$ to $\langle T_s' \rangle$ in this region yields $m \approx 2.7$. The derived value is smaller although close enough to indicate that most of the processes are qualitatively

captured. The QTCM budgets indicate that \mathbf{v}' effects in moisture advection and evaporation are not actually negligible, and we infer that this is the cause of error in the derived estimate of m .

References

- Angell, J. K., 1981: Comparison of variations in atmospheric quantities with sea surface temperature variations in the equatorial eastern Pacific. *Mon. Wea. Rev.*, **109**, 230-243.
- Chou, C., 1997: Simplified radiation and convection treatments for large-scale tropical atmospheric modeling. Ph.D. Dissertation, University of California, Los Angeles, 215pp.
- Chou, C., J. D. Neelin and H. Su, 2001: Ocean-atmosphere-land feedbacks in an idealized monsoon. *Quart. J. Roy. Meteor. Soc.*, **127**, 1869–1891.
- Gill, A. E., 1980: Some simple solutions for heat induced tropical circulation. *Quart. J. Roy. Meteor. Soc.*, **106**, 447–462.
- Horel, J. D., and J. M. Wallace, 1981: Planetary-scale atmospheric phenomena associated with the Southern Oscillation. *Mon. Wea. Rev.*, **109**, 813–829.
- Lau, N.-C., 1985: Modeling the seasonal dependence of the atmospheric response to observed El Niños in 1962-76, *Mon. Wea. Rev.*, **113**, 1970–1996.
- Lau, N.-C., and M. J. Nath, 2001: Impact of ENSO on SST variability in the north Pacific and north Atlantic: seasonal dependence and role of extratropical sea-air coupling. *J. Climate*, **14**, 2846–2866.
- Lin, J. W.-B., J. D. Neelin, and N. Zeng, 2000: Maintenance of tropical variability: Impact of evaporation-wind feedback and midlatitude storms. *J. Atmos. Sci.*, **57**, 2793–2823.
- Kalnay, E., et al., 1996: The NCEP/NCAR 40-year reanalysis project. *Bull. Amer. Meteor. Soc.*, **77**, 437–471.
- Kiladis, G. N., and H. F. Diaz, 1989: Global climatic anomalies associated with extremes in the Southern Oscillation. *J. Climate*, **2**, 1069–1090.
- Kumar, A. and M. P. Hoerling, 1998: Specification of regional sea surface temperatures in the atmospheric general circulation model simulations, *J. Geophys. Res.*, **103**, 8901–8907.
- Kumar, A. and M. P. Hoerling, 2002: The Nature and causes for the delayed Atmospheric Response to El Niño, *J. Climate*,, *submitted*.
- Mechoso, C. R., A. Kitoh, S. Moorthi and A. Arakawa, 1987: Numerical simulations of the atmospheric response to a sea surface temperature anomaly over the equatorial eastern Pacific ocean. *Mon. Wea. Rev.*, **115**, 2936–2956.
- Neelin, J. D., and N. Zeng, 2000: A quasi-equilibrium tropical circulation model—formulation. *J. Atmos. Sci.*, **57**, 1741–1766.
- Newell, R. E., and B. C. Weare, 1976: Ocean temperatures and large scale atmospheric variations. *Nature*, **262**, 40–41.
- Pan, Y. H., and A. H. Oort, 1983: Global climate variations connected with sea surface

- temperature anomalies in the eastern equatorial Pacific Ocean for the 1958-73 Period. *Mon. Wea. Rev.*, **111**, 1244–1258.
- Reynolds, R. W., and T. M. Smith, 1994: Improved global sea surface temperature analyses using optimum interpolation, *J. Climate*, **7**, 929–948.
- Sobel, A. H. and C. S. Bretherton, 2000: Modeling Tropical precipitation in a single column. *J. Climate*, **13**, 4378–4392.
- Sobel, A. H., I. M. Held, and C. S. Bretherton, 2002: The ENSO signal in tropical tropospheric temperature. *J. Climate*, *Accepted*.
- Spencer, R. W., and J. R. Christy, 1992: Precision and Radiosonde Validation of Satellite Grid-point Temperature Anomalies. Part II: A Tropospheric Retrieval and Trends during 1979–90. *J. Climate*, **5**, 858–866.
- Su, H., J. D. Neelin, and C. Chou, 2001: Tropical teleconnection and local response to SST anomalies during the 1997-1998 El Niño. *J. Geophys. Res.*, **106**, 20,025–20,043
- Su, H., and J. D. Neelin, 2002: Teleconnection mechanisms for tropical Pacific descent anomalies during El Niño. *J. Atmos. Sci.*, **59**, 2682-2700.
- Sun, D. Z., and I. M. Held, 1996: A comparison of modeled and observed relationships between interannual variations of water vapor and temperature. *J. Climate*, **9**, 665–675.
- Sun, D. Z., and A. H. Oort, 1995: Humidity-temperature relationships in the tropical troposphere. *J. Climate*, **8**, 1974–1987.
- Trenberth, K. E., G. W. Branstator, D. Karoly, A. Kumar, N.-C. Lau and C. Ropelewski, 1998: Progress during TOGA in understanding and modeling global teleconnections associated with tropical sea surface temperatures. *J. Geophys. Res.*, **103**, 14,291–14,324.
- Xie, P., and P.A. Arkin, 1997: Global precipitation: A 17-year monthly analysis based on gauge observations, satellite estimates and numerical model outputs, *Bull. Amer. Meteor. Soc.*, **78**, 2539–2558.
- Zeng, N., and J. D. Neelin, 2000: The role of vegetation-climate interaction and interannual variability in shaping the African Savanna. *J. Climate*, **13**, 2665–2670
- Zeng, N., J. D. Neelin, and C. Chou, 2000: A quasi-equilibrium tropical circulation model—implementation and simulation. *J. Atmos. Sci.*, **57**, 1767–1796.

Table 1: Examples from the analytical model of the slope α of tropical averaged tropospheric temperature anomaly versus tropical averaged SST anomaly. The first four cases correspond to regional SST anomaly experiments. The OBS-SST case correspond to linearizing about values approximated for the OBS-SST run in section 3. The last three cases correspond to changing one parameter at a time relative to the OBS-SST case. See text for details. For all cases, $(\overline{V}_s)_{trop} = 5.5ms^{-1}$. The SST anomaly shape factor σ is defined in (8.9). The values of γ are given for moisture in temperature units so γ is non-dimensional.

	$(\overline{V}_s)_{region}(ms^{-1})$	$\gamma@T_s(K)$	σ	α
Pac 1 (P)	6.0	3.5 @ 302	0	1.9
Pac 3 (P)	6.5	3.0 @ 299	0.1	1.7
Pac 4 (P)	6.5	3.0 @ 299	0.4	1.4
SE Pac (NP)	7.5	2.5 @ 293	1.0	0.6
OBS-SST	5.5	3.2 @ 300	0.25	1.4
WARM-SST	5.5	3.5 @ 302	0.25	1.5
HIGH-V	7.5	3.2 @ 300	0.25	1.9
ALL-P	5.5	3.2 @ 300	0.0	1.7

Figure Captions

Figure 1. Tropical averaged (25S-25N) tropospheric temperature anomalies versus tropical averaged SST anomalies for the NCAR/NCEP reanalysis (1982-1998), the MSU temperature (1982-1993) and the QTCM simulation using observed SST from 1982-1998. The solid lines are the linear fits to the three datasets. The slopes of three lines are shown in the upper-left corner.

Figure 2. Observed anomalies for January-March 1998. (a) sea surface temperature (SST) in

C, (b) precipitation (contoured at -10, -8, -6, -4, -2, -1, 1, 2, 4, 6, 8, 10 mm/day, dark shading for positive values and light shading for negative values) and (c) tropospheric temperature (850-200 hPa average; contour interval 0.5 C, light shading between 0.5 and 1, dark shading above 1).

Figure 3. As in Fig. 2 but for November 1994 - January 1995. Shading in (c) above 0.

Figure 4. Model-simulated (a) precipitation (mm/day) and (b) tropospheric temperature (850-200hPa average, in C) anomalies for JFM 1998 from the OBS-SST run. The precipitation anomalies are contoured at -2, -1, -0.5, 0, 1, 2, 4 mm/day, dark shading above 1 and light shading below -0.5. The temperature anomalies are contoured at 0.25 C, dark shading above 0.75 and light shading between 0.25 and 0.75.

Figure 5. As in Fig. 4 but for NDJ 1994-95. Shading in (b) above 0.

Figure 6. The QTCM response to positive SST anomalies during JFM 1998. The JFM positive-only portion of the SST anomalies are specified in the region indicated by a dark outline. (a) Precipitation anomaly (mm/day), and (b) Tropospheric temperature anomalies (850-200hPa average, in C). Contour and shading same as Fig. 4.

Figure 7. The sum of the QTCM response to each of the four subregions of positive SST anomalies during JFM 1998. The four subregions are indicated by dark outlines. (a) Precipitation anomaly (mm/day). (b) Tropospheric temperature anomalies (850-200hPa average, in C). Contour and shading same as Fig. 4.

Figure 8. The QTCM response to one of the four subregions of positive SST anomalies during JFM 1998. The subregion is indicated by a dark outline. (a) Precipitation anomaly (mm/day). (b) Tropospheric temperature anomalies (850-200hPa average, in C). Note the temperature anomalies contoured at -0.025, 0, 0.025, 0.05, 0.1, and 0.15 C, with light shading between 0.025 and 0.05 and dark shading above 0.1.

Figure 9. The QTCM response to a small subregion of positive SST anomalies taken from

the JFM 1998 El Niño case. The subregion is indicated by a dark outline. (a) Precipitation anomaly (mm/day). (b) Tropospheric temperature anomalies (850-200hPa average, in C). Note the temperature anomalies contoured at -0.2, -0.1, 0, 0.025, 0.1, 0.2, and 0.3 C, with shadings starting above 0.025.

Figure 10. (a) Tropical averaged (25S-25N) tropospheric temperature anomalies versus the spatial integral of SST anomaly forcing for a number of experiments with subregions of the 1998 JFM El Niño SST anomaly. The side-panels show examples of the SST anomaly forcing used in the experiments. (b) Tropical averaged (25S-25N) precipitation anomalies versus the spatial integral of SST anomaly forcing for the same experiments as in (a). The side-panels show examples of the spatial distribution of precipitation anomalies over the entire tropical band.

Figure 11. Tropical averaged (25S-25N) (a) tropospheric temperature anomalies and (b) precipitation anomalies versus tropical averaged SST anomalies for simulations with uniform SST anomalies of amplitude -5 C to 5 C added to climatological SST in three subregions. The regions are indicated by outlines in (c) and marked 1, 3 and 4 based on the four subregion experiments for the JFM 1998 El Niño. Open points show results of the experiments. Linear fits to small SST anomaly values (-0.5 C to 0.5 C) are extrapolated as thin lines. The observed SST anomaly range within each subregion is indicated by thicker lines. The numbers next to the linear fits are the corresponding slopes α . (c) Climatological precipitation during JFM.

Figure 12. Same as Fig. 11 but for experiments over a climatologically non-precipitating region, as indicated by dark outline in the climatological precipitation map (c). In (b), numbers next to the dots are the amplitudes of SST anomalies used in the subregion, and the linear fit uses all SST anomaly experiments.

Figure 13. Two measures of the sensitivity parameter of tropical-average tropospheric temperature to SST anomaly in each of four subregions of the 1998 JFM positive SST anomalies (a) and the NDJ 1994-1995 case (b). The upper numbers are the amount of

tropospheric temperature anomalies in degree C per unit SST forcing in ($C10^{12}m^2$) (amplitude x area). The lower numbers are the fraction of the average tropospheric temperature anomaly contributed by each subregion.

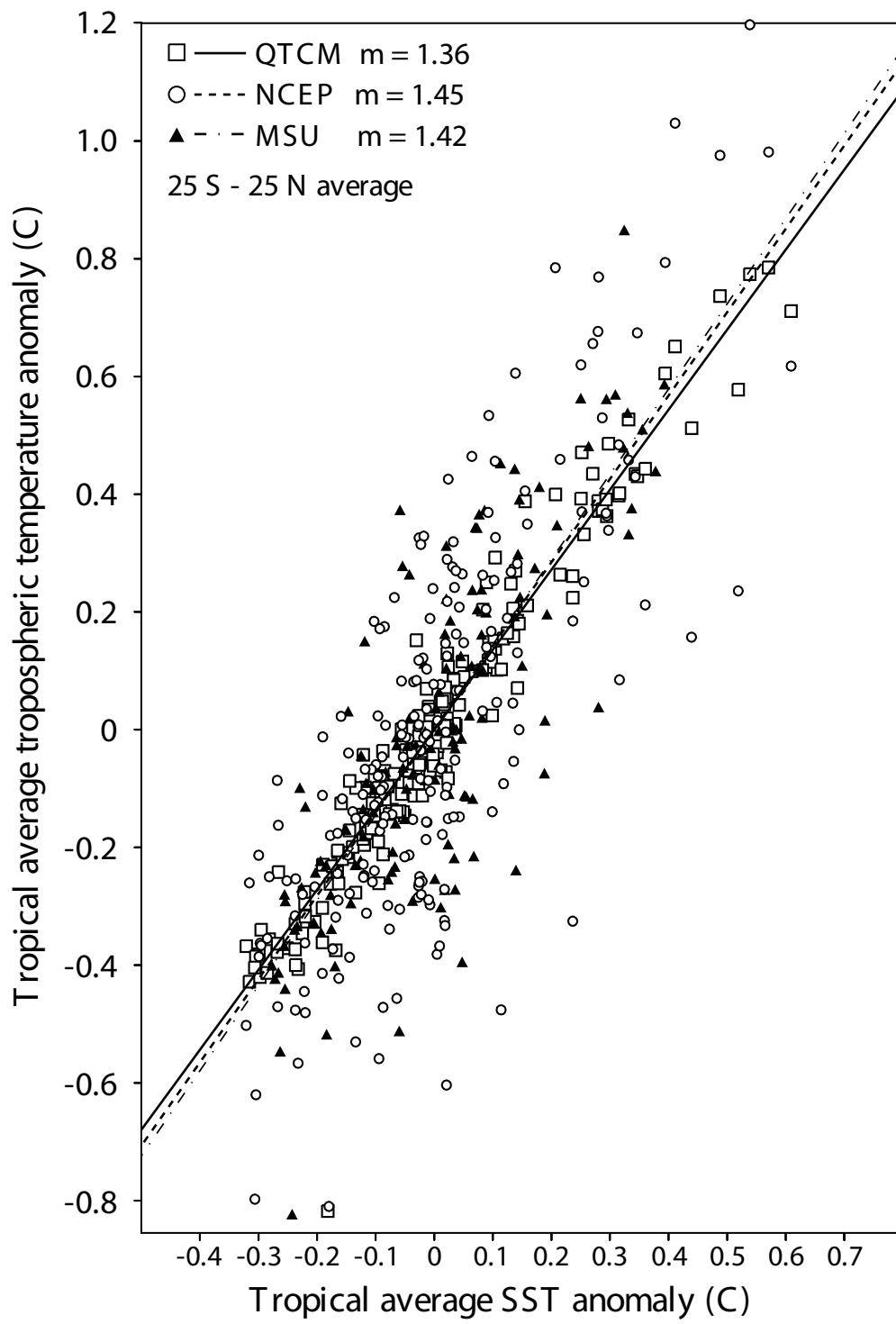


Fig. 1

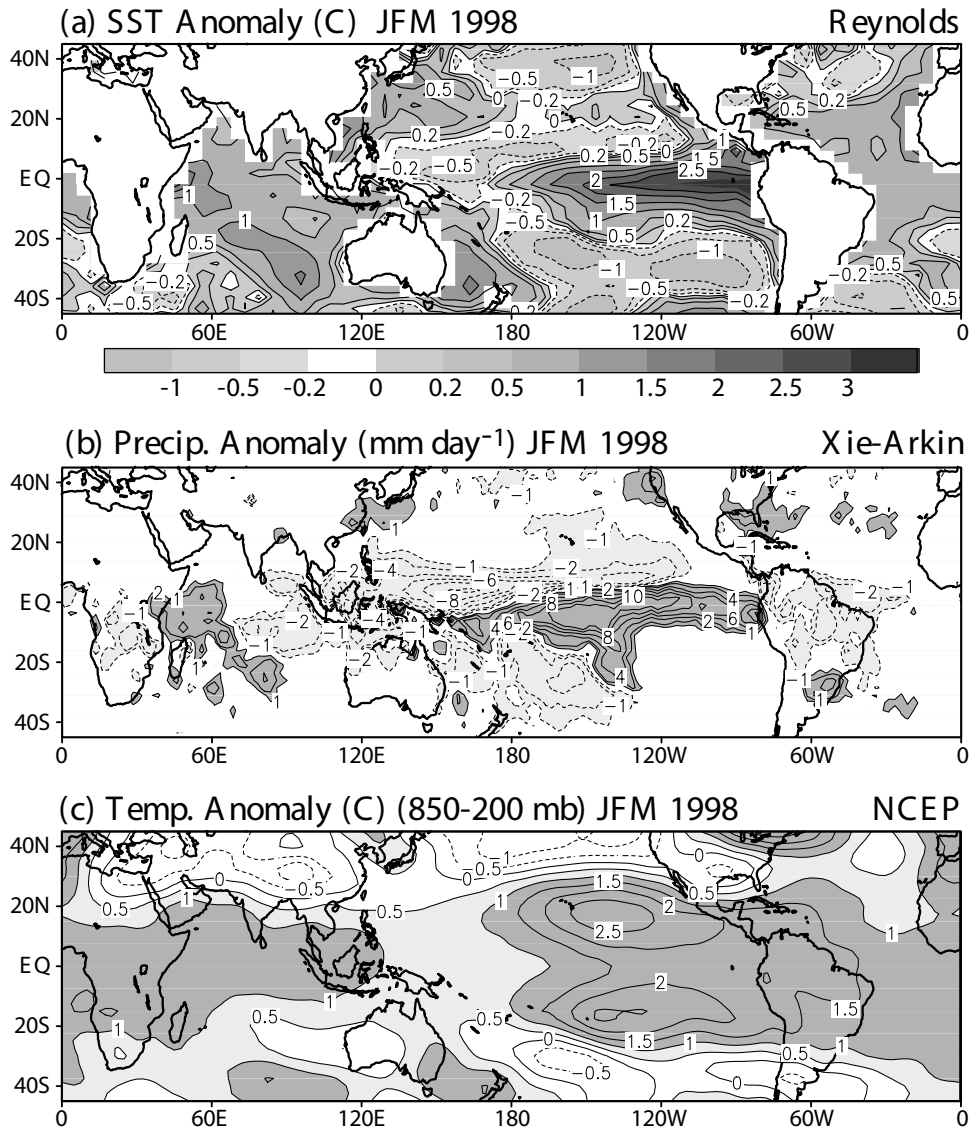


Fig. 2

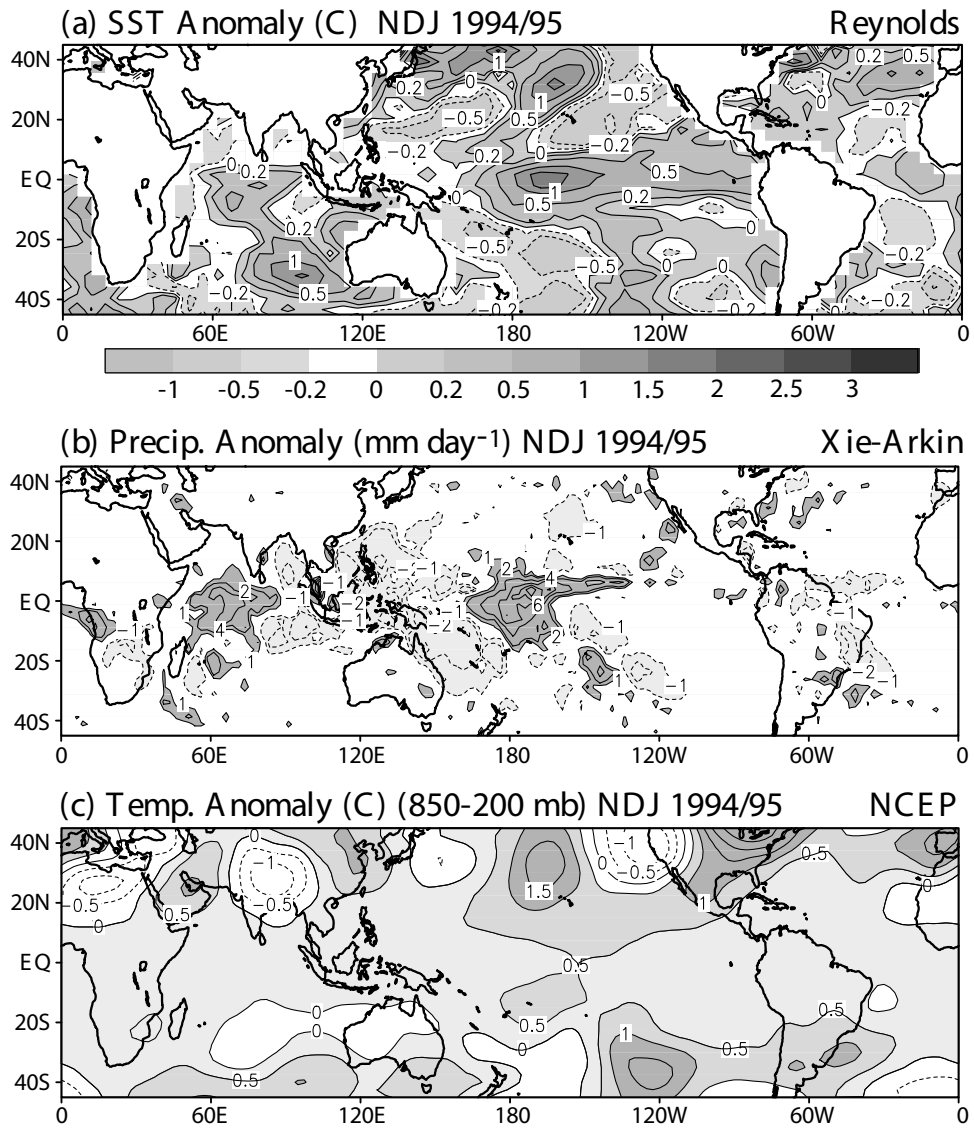
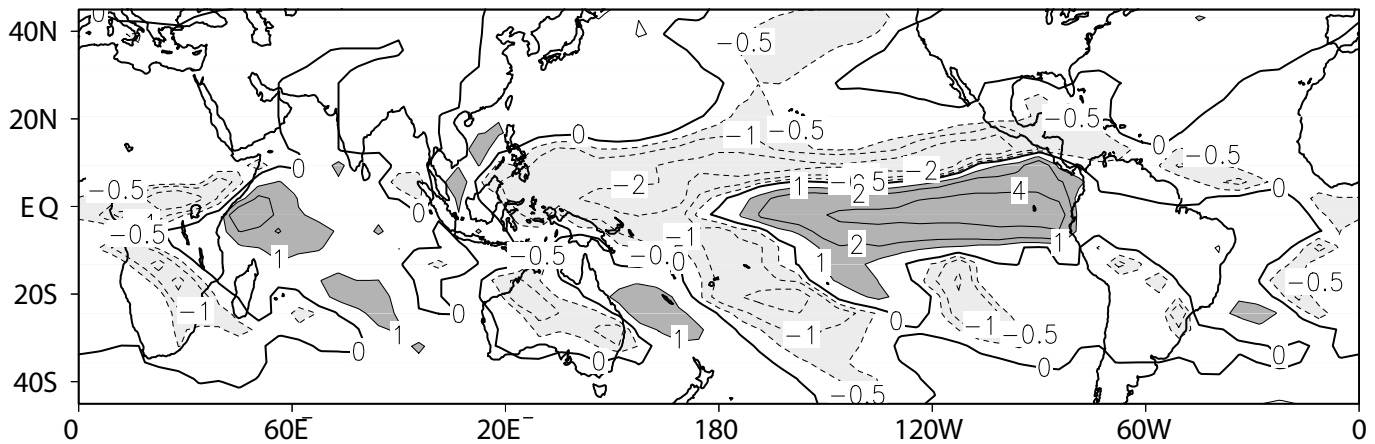


Fig. 3

(a) Precip. Anomaly JFM 1998



(b) Temp. Anomaly (850 - 200 hpa) JFM 1998

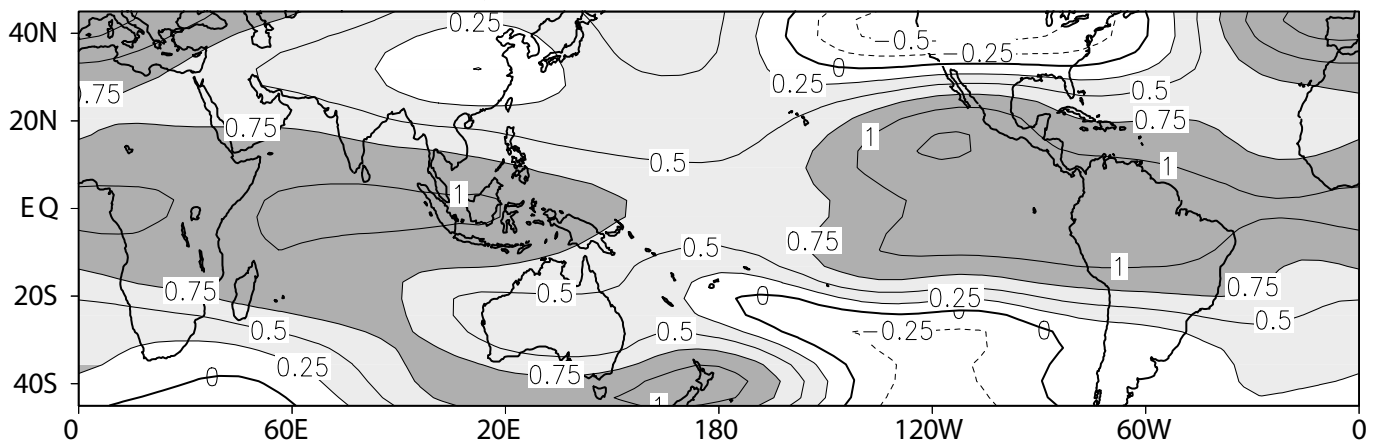
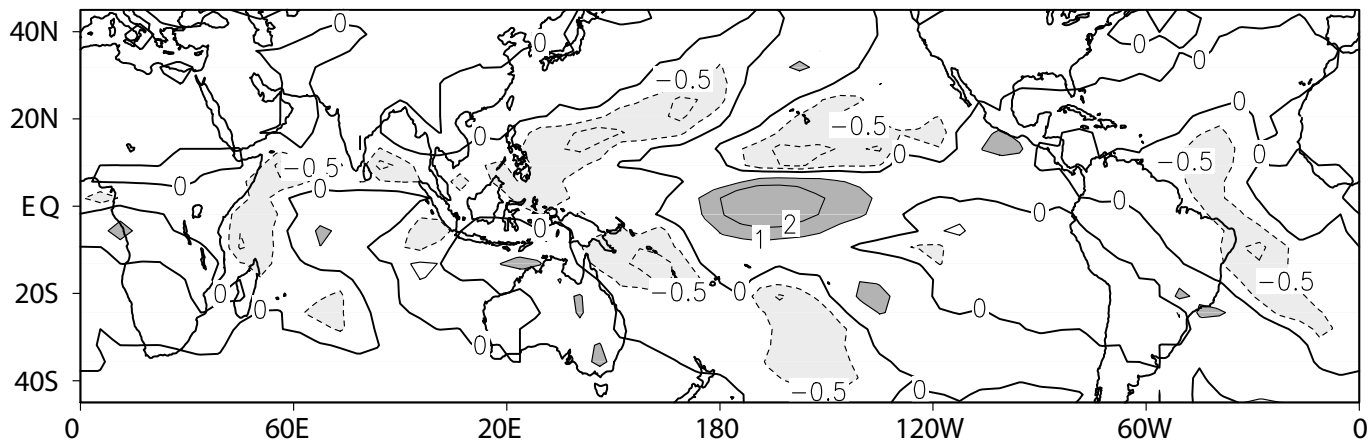


Fig.4

(a) Precip. Anomaly DJF 1994/95



(b) Temp. Anomaly (850 - 200 hpa) DJF 1994/95

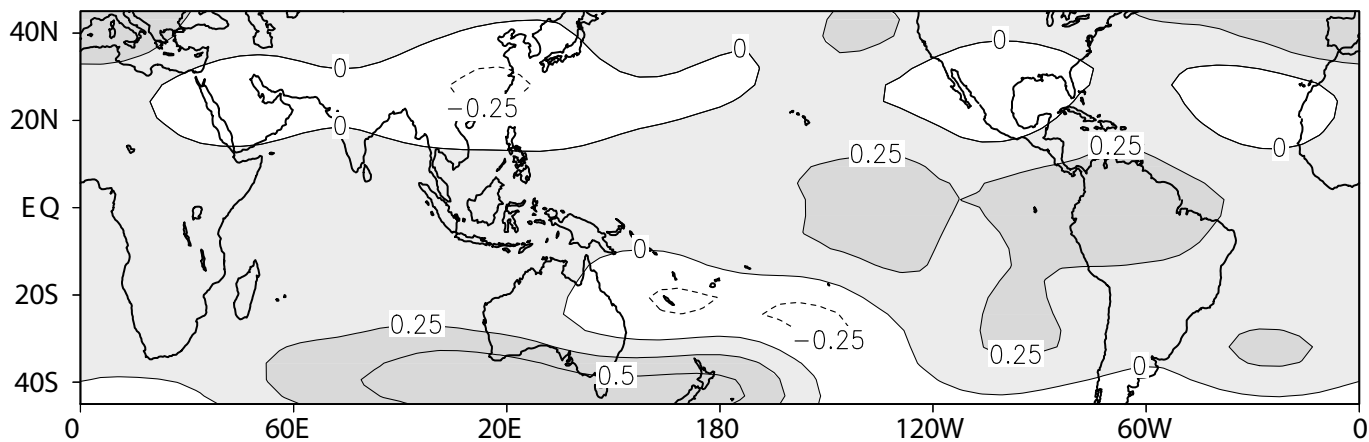
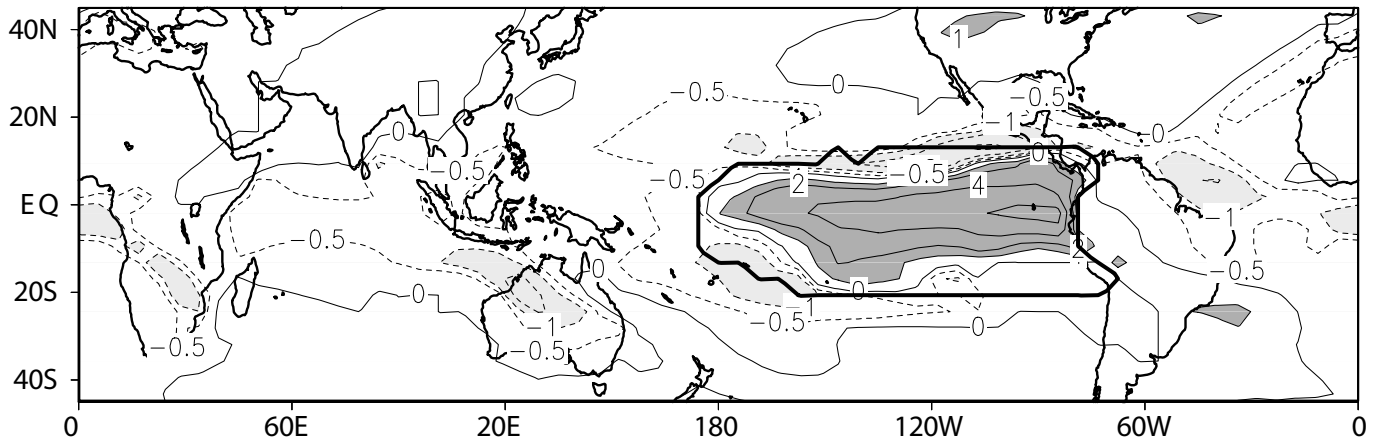


Fig. 5

(a) Precip. JFM 1998 ENSOPAC - CLIM



(b) Temp. (850 - 200 hpa) JFM 1998 ENSOPAC - CLIM

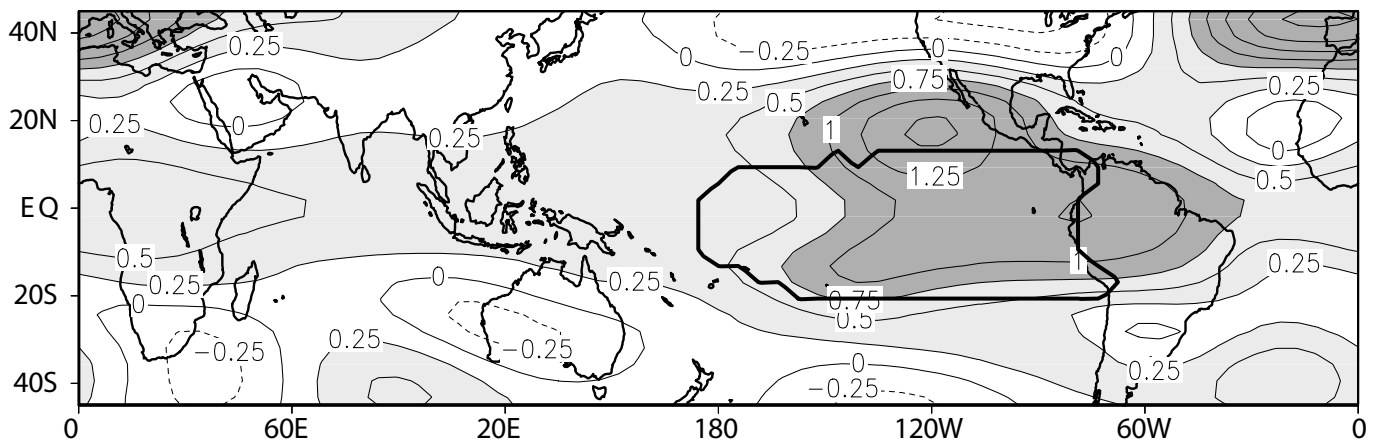
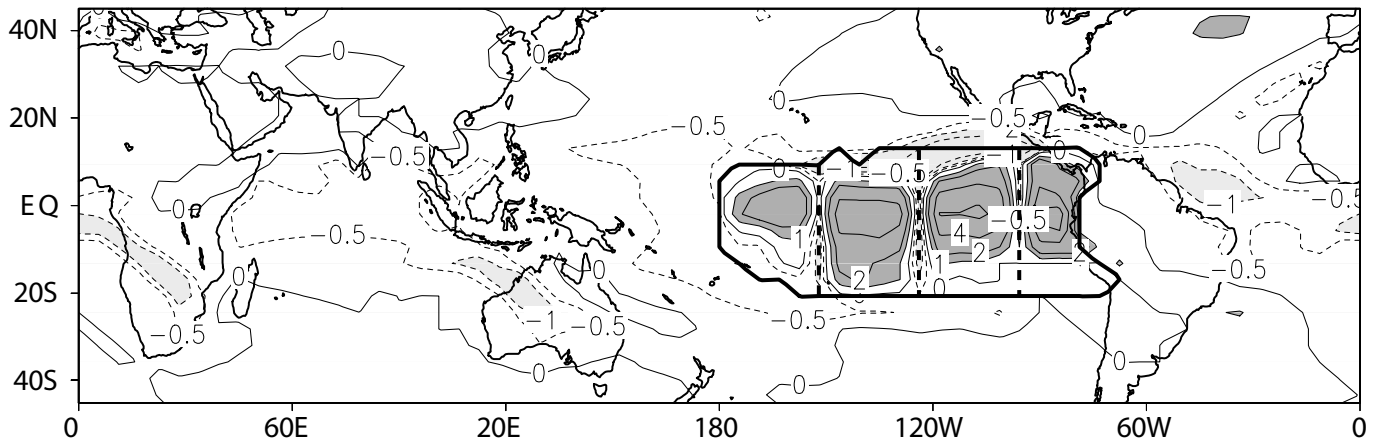


Fig. 6

(a) Precip. JFM 1998 ENSOPAC_SUM - CLIM



(b) Temp. (850 - 200 hpa) JFM 1998 ENSOPAC_SUM - CLIM

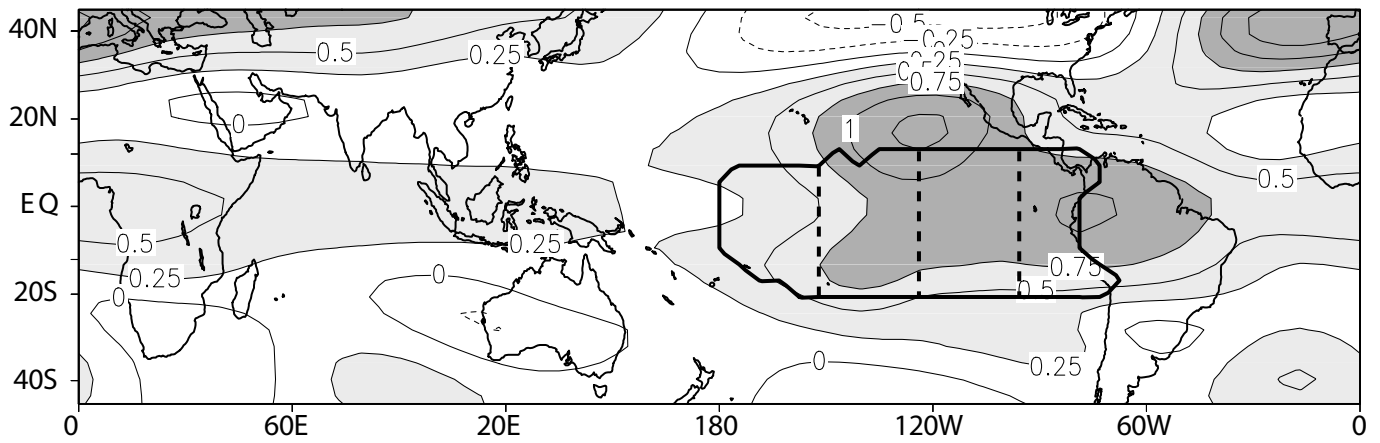
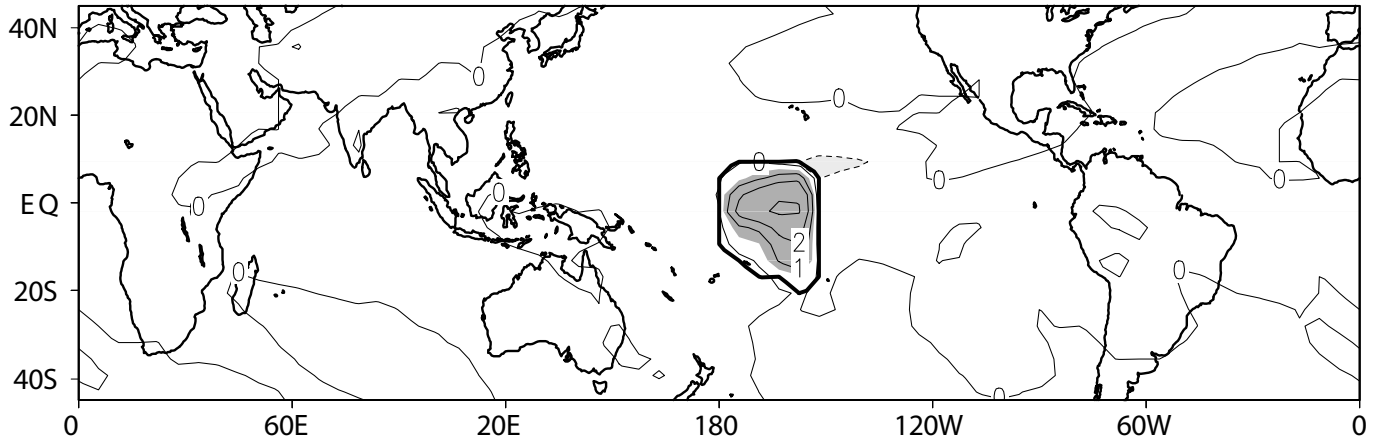


Fig. 7

(a) Precip. JFM 1998 ENSOPAC_1 - CLIM



(b) Temp. (850 - 200 hpa) JFM 1998 ENSOPAC_1 - CLIM

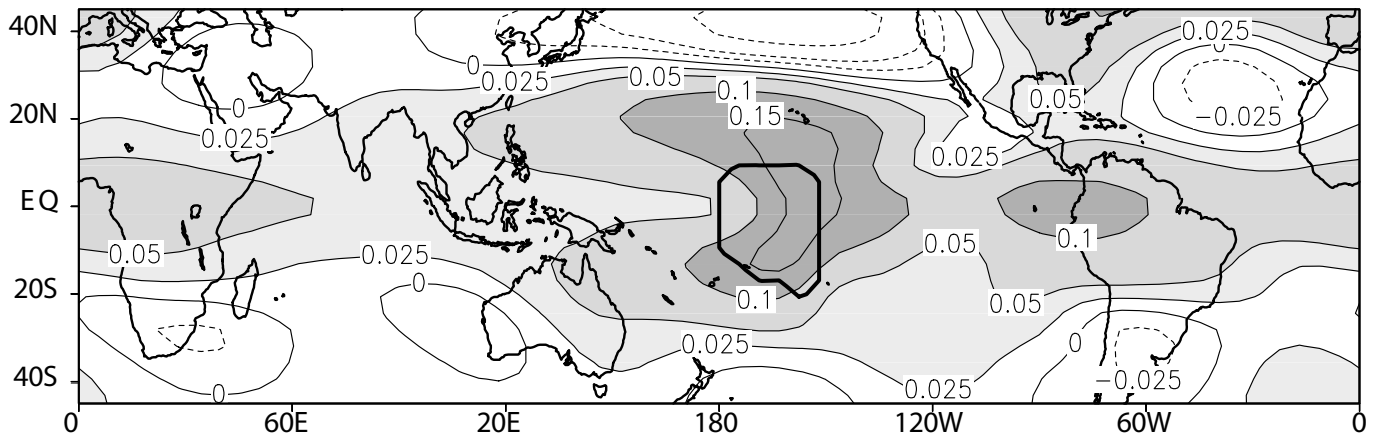
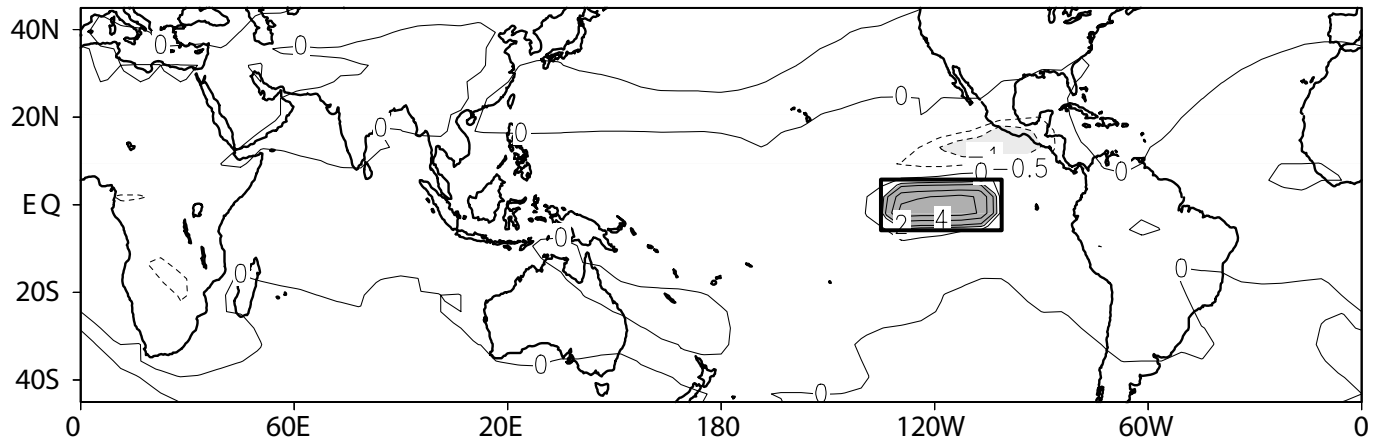


Fig 8

(a) Precip. JFM 1998 ENSOPAC_L2b- CLIM



(b) Temp. (850 - 200 hpa) JFM 1998 ENSOPAC_L2b- CLIM

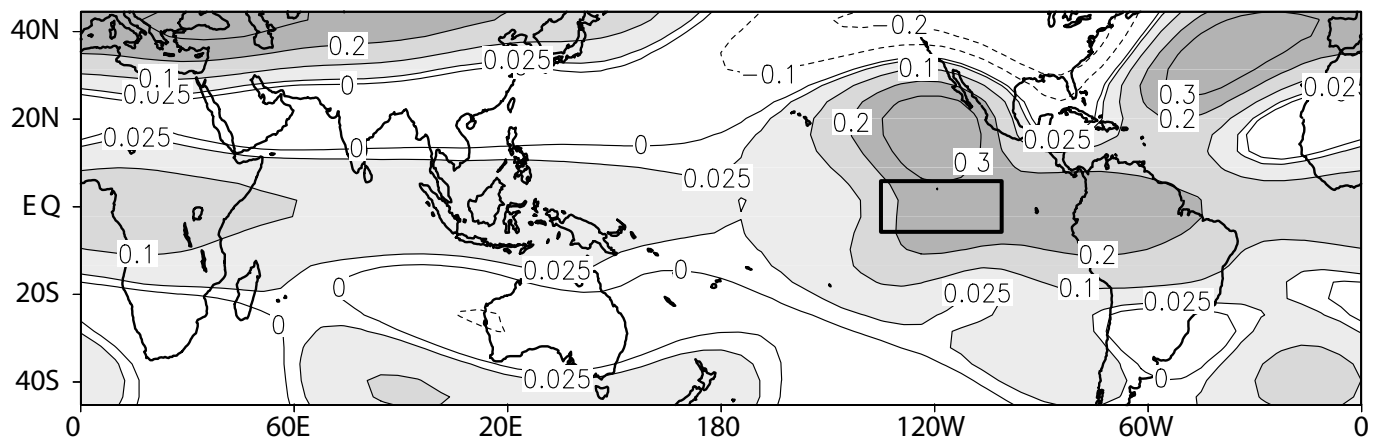


Fig. 9

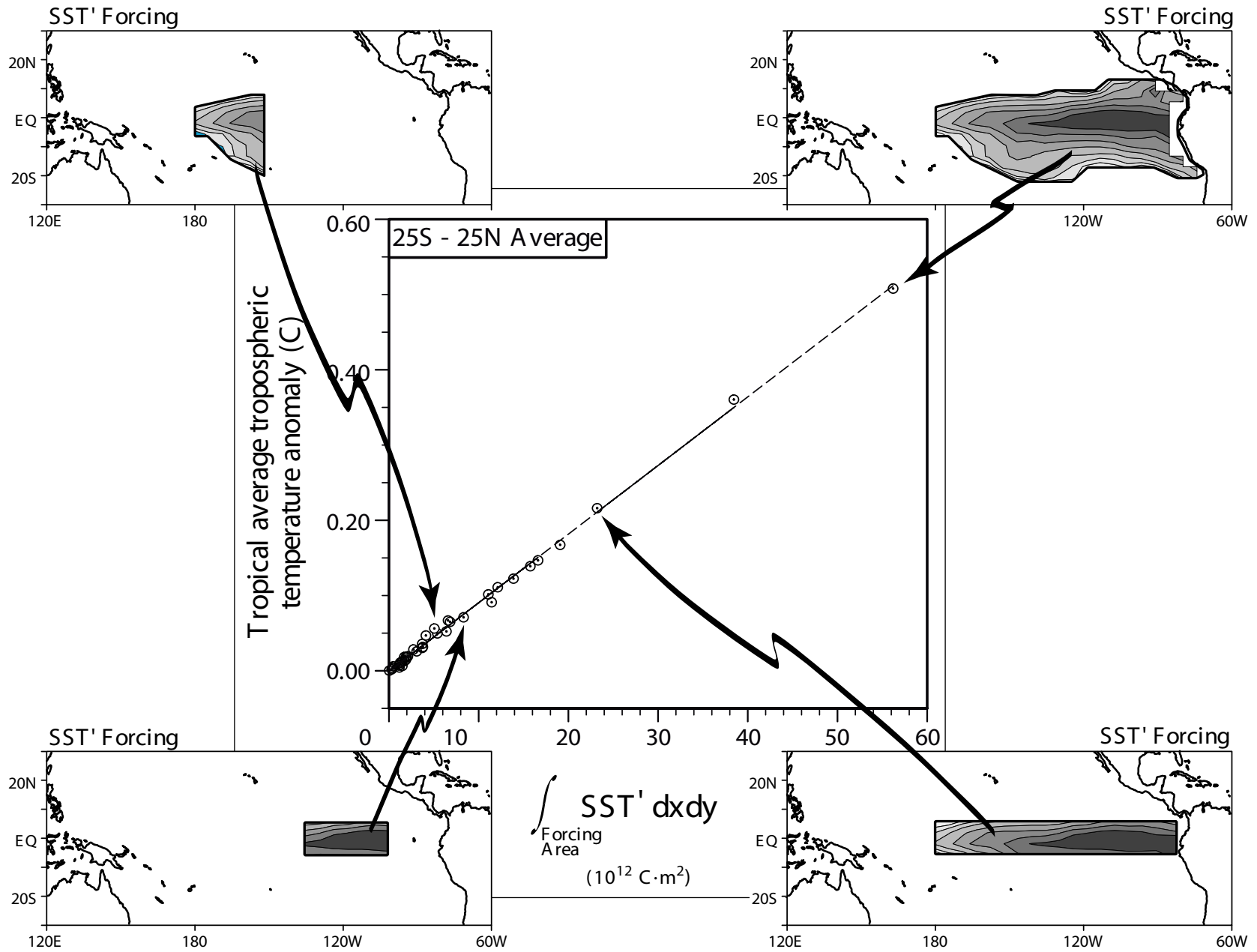


Fig. 10a

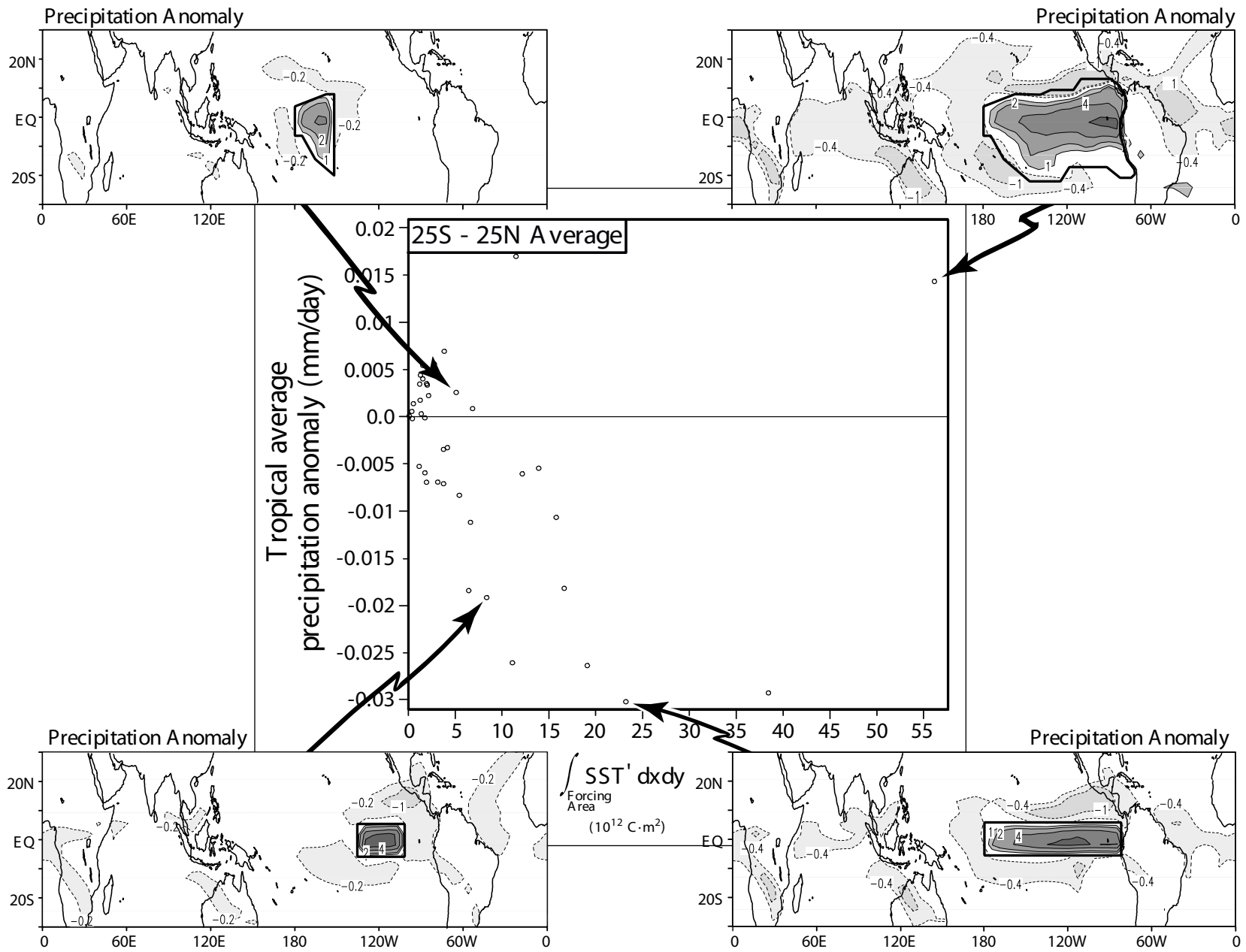


Fig. 10b

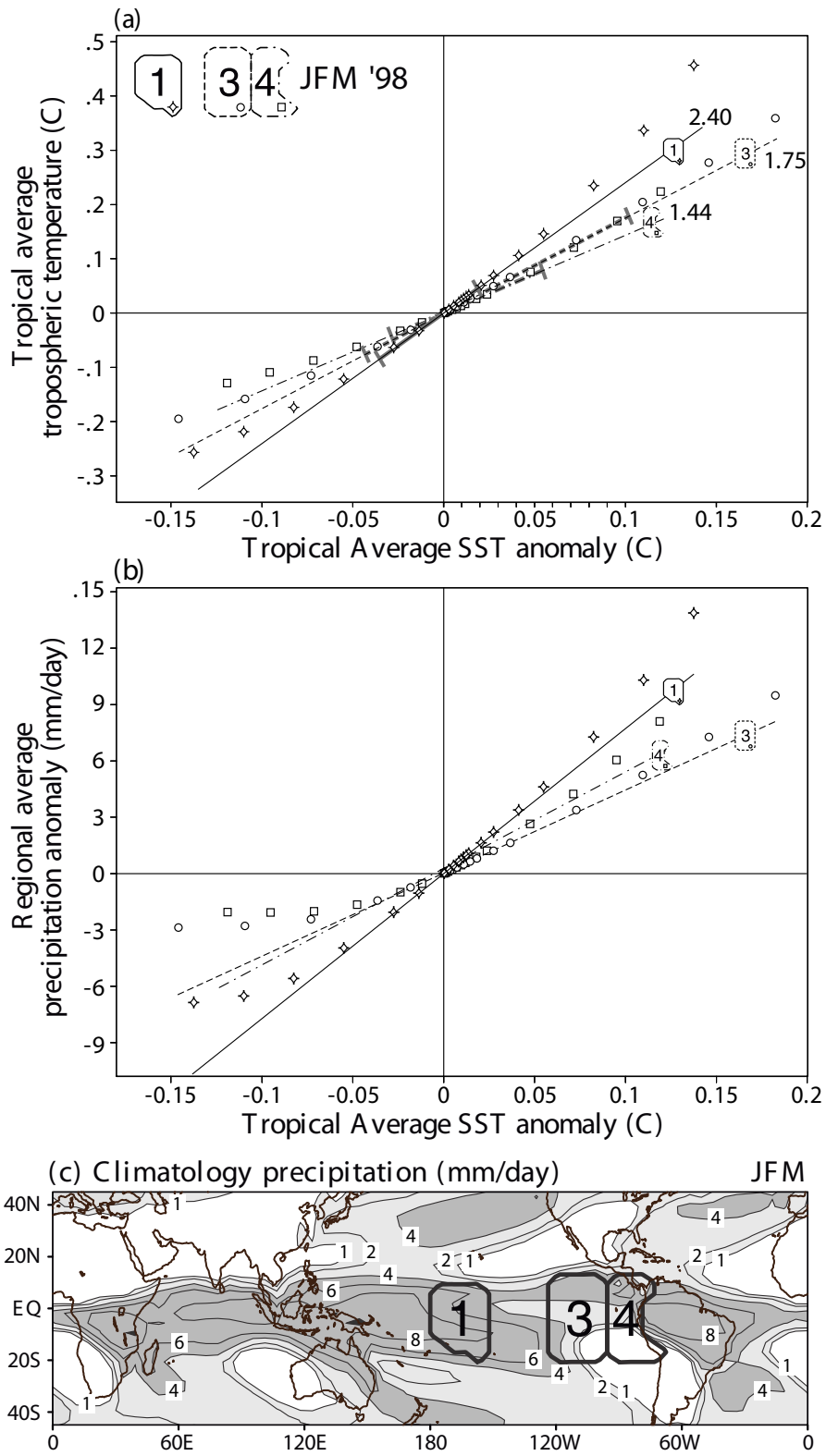


Fig. 11

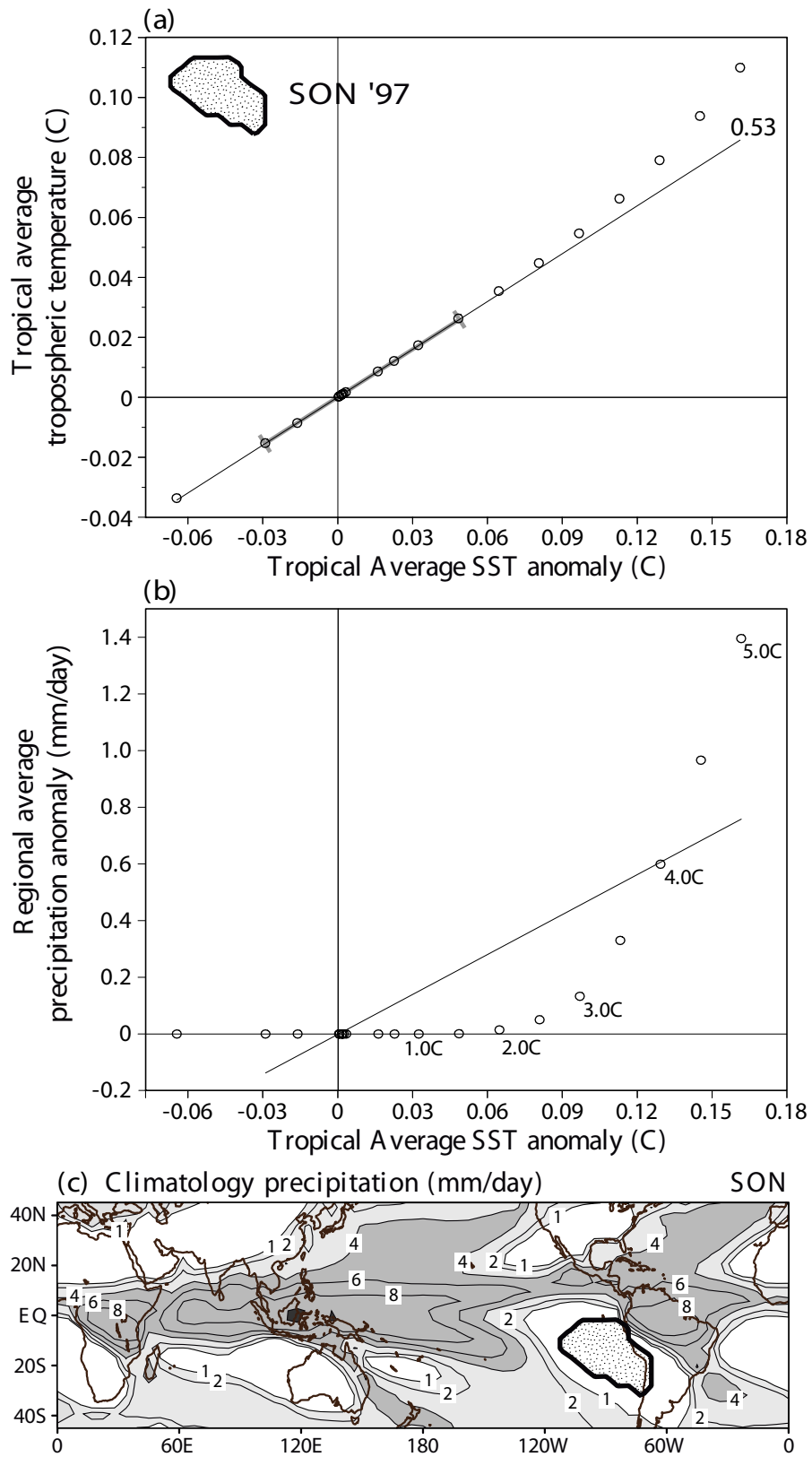


Fig. 12

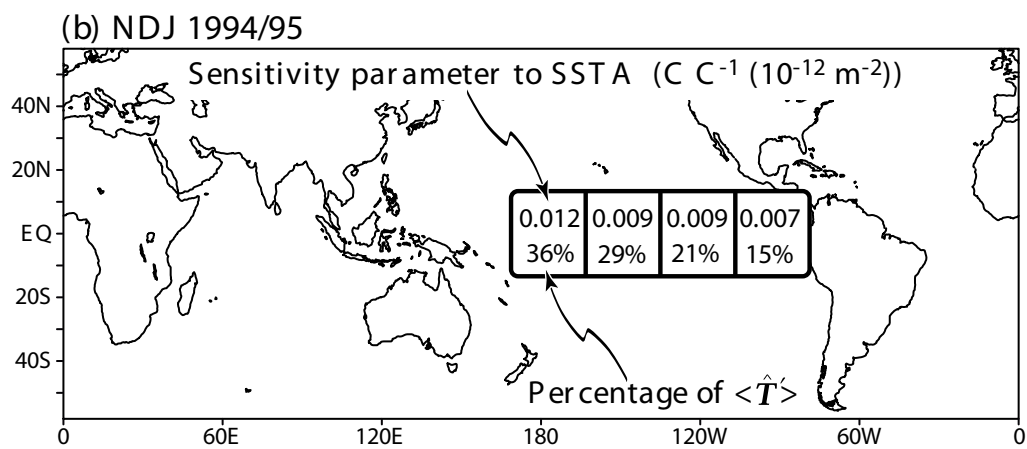
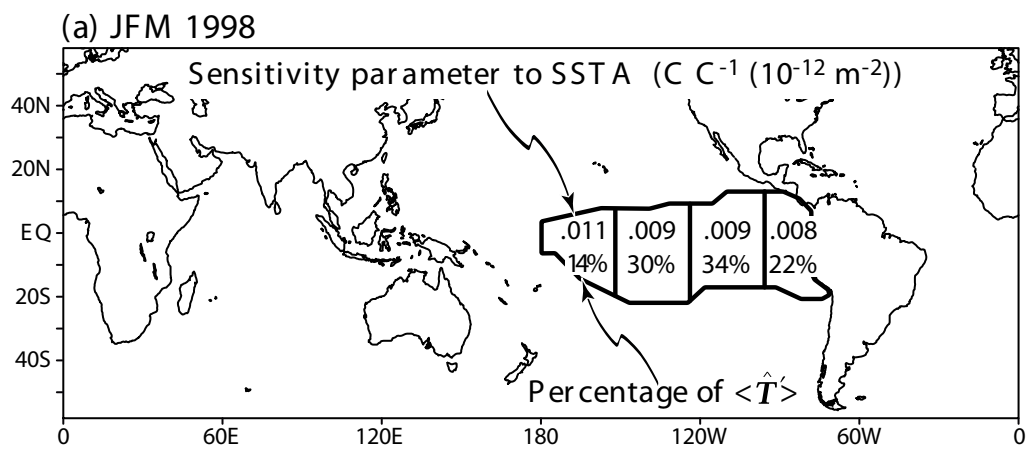


Fig. 13